



Deglacial carbon cycle changes observed in a compilation of 117 benthic $\delta^{13}\text{C}$ time series (20-6 ka)

Carlye Peterson^{1,2} and Lorraine Lisiecki²

¹Department of Earth Sciences, University of California Riverside, Riverside, California, USA.

²Department of Earth Science, University of California Santa Barbara, Santa Barbara, California, USA.

Correspondence: CARLYE PETERSON (CARLYE.PETERSON@GMAIL.COM)

Abstract. We present a compilation of 117 time series $\delta^{13}\text{C}$ records from *Cibicides wuellerstorfi* spanning the last deglaciation (20-6 kyr) and well-suited for reconstructing large-scale carbon cycle changes, especially for comparison with isotope-enabled carbon cycle models. The age models for the $\delta^{13}\text{C}$ records are derived from regional planktic radiocarbon compilations (Stern and Lisiecki, 2014). The $\delta^{13}\text{C}$ records were stacked in nine different regions and then combined using volume-weighted averages to create intermediate, deep, and global $\delta^{13}\text{C}$ stacks. These benthic $\delta^{13}\text{C}$ stacks are used to reconstruct mean changes in the size of the terrestrial biosphere and deep ocean carbon storage. The timing of change in global mean $\delta^{13}\text{C}$ is interpreted to indicate terrestrial biosphere expansion from 19-6 ka. The $\delta^{13}\text{C}$ gradient between the intermediate and deep ocean, which we interpret as a proxy for deep ocean carbon storage, matches the pattern of atmospheric CO_2 change observed in ice core records. The presence of signals associated with the terrestrial biosphere and atmospheric CO_2 indicates that the compiled $\delta^{13}\text{C}$ records have sufficient spatial coverage and time resolution to accurately reconstruct large-scale carbon cycle changes during the glacial termination.

Copyright statement.

1 Introduction

On glacial-interglacial timescales, carbon cycle changes redistribute the amount of carbon stored in the deep ocean, atmosphere and terrestrial biosphere (*e.g.*, Broecker (1982); Siegenthaler et al. (2005)). For example, as atmospheric CO_2 increased across the deglaciation, atmospheric $\delta^{13}\text{C}$ decreased, likely due to the ventilation of respired, ^{13}C -depleted carbon from the deep ocean (*e.g.*, Schmitt et al. (2012); Eggleston et al. (2016)). However, identifying the biogeochemical mechanisms associated with these carbon transfers is complicated by a variety of carbon cycle feedbacks (*e.g.*, Archer et al. (2000); Sigman and Boyle (2000); Peacock et al. (2006); Toggweiler et al. (2006); Kohfeld and Ridgwell (2009); Brovkin et al. (2012); Menviel et al. (2012); Galbraith and Jaccard (2015); Buchanan et al. (2016)). This study seeks to improve our understanding of glacial-interglacial carbon cycle changes by reconstructing changes in mean ocean $\delta^{13}\text{C}$ and its vertical gradient and comparing the results with changes in the terrestrial biosphere and atmospheric CO_2 .



The $\delta^{13}\text{C}$ of benthic foraminiferal calcite is a well-established carbon cycle proxy, which records the $\delta^{13}\text{C}$ signature of the dissolved inorganic carbon (DIC) in seawater at seafloor depths (*e.g.*, Woodruff and Savin (1985); Zahn et al. (1986); Lutze and Thiel (1989); Duplessy et al. (1988); Mackensen (2008); Gottschalk et al. (2016); Schmittner et al. (2017)). Averages of benthic foraminiferal $\delta^{13}\text{C}$ time series, called stacks, can improve the signal-to-noise ratio of regional or global seawater changes (*e.g.*, Lisiecki et al. (2008); Lisiecki (2014)). Global mean benthic $\delta^{13}\text{C}$ change is likely caused by changes in terrestrial organic carbon storage (Shackleton, 1977; Curry et al., 1988; Duplessy et al., 1988; Ciais et al., 2012; Peterson et al., 2014), while vertical $\delta^{13}\text{C}$ gradients may record changes in deep ocean carbon storage and atmospheric CO_2 (Oppo and Fairbanks, 1990; Flower et al., 2000; Hodell et al., 2003; Lisiecki, 2010). The vertical $\delta^{13}\text{C}$ gradient between the surface (high $\delta^{13}\text{C}$) and deep ocean (low $\delta^{13}\text{C}$) primarily results from the accumulation of low- $\delta^{13}\text{C}$ respired organic carbon in deep water, which temporarily sequesters it from the atmosphere. Conversely, vertical mixing of the ocean will tend to ventilate deep ocean carbon to the surface ocean and atmosphere while simultaneously decreasing the vertical $\delta^{13}\text{C}$ gradient. Therefore, the vertical $\delta^{13}\text{C}$ gradient likely records changes in deep ocean carbon storage, which is an important factor controlling glacial-interglacial changes in atmospheric CO_2 (*e.g.*, Schmitt et al. (2012); Eggleston et al. (2016)).

Here we compile and analyze 117 high-resolution benthic $\delta^{13}\text{C}$ records from the Atlantic, Pacific, and Indian Oceans spanning the last deglaciation to investigate changes in both the ocean and terrestrial biosphere components of the global carbon cycle. Benthic $\delta^{13}\text{C}$ records are combined into regional stacks, which are then used to construct time series of volume-weighted global mean $\delta^{13}\text{C}$ and the vertical $\delta^{13}\text{C}$ gradient between intermediate and deep waters.

We analyze these stacks to test the following hypotheses:

1. The deglacial pattern of global mean ocean $\delta^{13}\text{C}$ change is a proxy for changes in the size of the terrestrial biosphere. If so, global mean $\delta^{13}\text{C}$ should continue to increase after atmospheric CO_2 levels plateau at 11 ka due to the slower response times for ice sheet retreat and ecosystem change (*e.g.*, Hoogakker et al. (2016); Davies-Barnard et al. (2017)). We compare the reconstructed global mean $\delta^{13}\text{C}$ change with several carbon cycle model estimates of terrestrial biosphere change. Additionally, we evaluate whether deep Pacific $\delta^{13}\text{C}$ correlates with global mean $\delta^{13}\text{C}$ change as previously assumed (Shackleton et al., 1983; Curry and Oppo, 1997; Lisiecki et al., 2008). This study provides the first opportunity to compare time series of deep Pacific $\delta^{13}\text{C}$ with a volume-weighted global mean $\delta^{13}\text{C}$ stack.
2. Changes in the vertical $\delta^{13}\text{C}$ gradient should closely resemble time series of atmospheric CO_2 if the deglacial CO_2 increase is caused by a decrease in deep ocean carbon storage. This hypothesis is supported by findings on orbital timescales using a smaller number of sites (Oppo and Fairbanks, 1990; Flower et al., 2000; Hodell et al., 2003; Lisiecki, 2010), but the link between the vertical $\delta^{13}\text{C}$ gradient and CO_2 has not yet been evaluated at millennial timescales or using a global data compilation. Observing such a link would improve our understanding of deglacial atmospheric CO_2 increase and, furthermore, demonstrate that the data compilation presented here has adequate spatial and temporal resolution with sufficiently precise age models to reconstruct millennial-scale changes in global benthic $\delta^{13}\text{C}$.



2 BACKGROUND

2.1 Benthic $\delta^{13}\text{C}$ reconstructions

Measurements of $\delta^{13}\text{C}$ from the calcite tests of epibenthic foraminifera *Cibicides wuellerstorfi* and related species (Schweizer et al., 2009) are commonly used to trace the spatial distribution of nutrients and deep water masses as well as changes in ocean carbon cycling (e.g., Curry et al. (1988); Duplessy et al. (1988); Curry and Oppo (2005); Schmittner et al. (2017)). However, the *Cibicides* species *C. kullenbergi* and *C. mundulus*, often measured in deep South Atlantic cores, appear to record more depleted $\delta^{13}\text{C}$ values than *C. wuellerstorfi* (Gottschalk et al., 2016).

Mean $\delta^{13}\text{C}$ change between the Last Glacial Maximum (LGM, 20 ka) and Late Holocene (6-0 ka) has been assessed with global compilations of *Cibicides wuellerstorfi* $\delta^{13}\text{C}$ records (e.g., Shackleton (1977); Duplessy et al. (1988); Curry et al. (1988); Boyle (1992); Matsumoto and Lynch-Stieglitz (1999); Curry and Oppo (2005); Herguera et al. (2010); Oliver et al. (2010); Hesse et al. (2011); Peterson et al. (2014); Gebbie et al. (2015)). These time slice studies include as many as 500 core sites, but generally undersample portions of the ocean with poor carbonate preservation, low primary productivity, and low sedimentation rates (i.e., the Southern Ocean south of 55S, the Indian Ocean, and the Pacific Ocean). In contrast, some portions of the Atlantic, especially the North Atlantic, are relatively well-sampled with abundant, well-preserved *C. wuellerstorfi*. Therefore, the time evolution of whole-ocean $\delta^{13}\text{C}$ is less well-constrained than Atlantic vertical, zonal, and meridional $\delta^{13}\text{C}$ gradients.

Because deglacial carbon cycle changes occur on millennial to centennial timescales, there is a need for a high resolution benthic $\delta^{13}\text{C}$ compilation of globally-distributed sites on a consistent age model across the glacial termination. Global compilations of $\delta^{13}\text{C}$ time series tend to focus on orbital-scale responses because their age models are not precise enough to analyze the relative timing of carbon cycle changes during the deglaciation (e.g., Lisiecki et al. (2008)). One global $\delta^{13}\text{C}$ data synthesis, which includes 258 records from many benthic and planktic foraminifera species, is not recommended for analyzing $\delta^{13}\text{C}$ changes on timescales of less than 10 kyr due to age model uncertainty and the inclusion of low-resolution records (Oliver et al., 2010). Studies of the last glacial termination often focus on local or regional depth transects that contain high-resolution $\delta^{13}\text{C}$ records with good age control (e.g., Sarnthein et al. (1994); Thornalley et al. (2010); Hoffman and Lund (2012); Tessin and Lund (2013); Lund et al. (2015); Oppo et al. (2015); Sikes et al. (2016)). In modeling studies, transient simulations are typically compared to a small number of individual benthic $\delta^{13}\text{C}$ records or regional syntheses, presumably due to the limitations of available global $\delta^{13}\text{C}$ compilations (e.g. Köhler et al. (2005); Brovkin et al. (2007); Köhler et al. (2010)).

2.2 Terrestrial biosphere and mean ocean $\delta^{13}\text{C}$

A portion of the additional carbon released from the deep ocean since the LGM was taken up by the terrestrial biosphere. The transfer of carbon between the terrestrial biosphere and the deep ocean affects the global mean value of benthic $\delta^{13}\text{C}$ because the mean $\delta^{13}\text{C}$ signature of the terrestrial biosphere is significantly more negative (approximately -25‰) than mean ocean $\delta^{13}\text{C}$ (approximately 0‰) (Shackleton, 1977). The change in global mean benthic $\delta^{13}\text{C}$ between the LGM and the Holocene is estimated to be $0.32\text{‰} \pm 0.20\text{‰}$ (Peterson et al., 2014; Gebbie et al., 2015), but the timing of mean benthic $\delta^{13}\text{C}$ change across the deglaciation is not well known.



5 Deglacial changes in terrestrial carbon storage (soils and vegetation) can be reconstructed in many ways, including terrestrial vegetation proxies and archives (*e.g.*, pollen, paleovegetation), carbon cycle models (*e.g.*, box models, inverse methods, dynamic global vegetation models, biomization methods, *etc.*), and proxies such as benthic $\delta^{13}\text{C}$, triple oxygen isotopes (Landais et al., 2007), and atmospheric carbonyl sulfide (Aydin et al., 2016). These methods produce estimates of change in terrestrial carbon storage between the LGM and Holocene that vary from 200-1900 PgC due to uncertainties and assumptions associated with each method (see discussion and citations within Peterson et al. (2014)).

10 Due to uncertainties in the total magnitude of change, here we focus on comparing the timing of changes in terrestrial carbon storage and global mean benthic $\delta^{13}\text{C}$. Models simulate rapid increases in terrestrial carbon storage from approximately 19-10 ka, followed by more gradual changes from 10-0 ka (Kaplan et al., 2002; Joos et al., 2004; Köhler et al., 2005). More recently, the potential effects of changes in poorly-constrained carbon reservoirs (beneath ice sheets and on continental shelves) were evaluated using deglacial simulations of biogeophysical and land carbon changes from the HadCM3 General Circulation Model (GCM). The model simulated a rapid increase in terrestrial carbon storage from 20-14 ka, different responses between 14-11 ka depending on the model scenario, and then steady, gradual change from 11-4 ka (Davies-Barnard et al., 2017).

15 Estimates of global mean benthic $\delta^{13}\text{C}$ are also used to remove global changes from individual $\delta^{13}\text{C}$ records in order to identify patterns of local or regional change, *e.g.*, related to ocean circulation. Because estimates of global mean $\delta^{13}\text{C}$ have only been available for the LGM and Holocene, some studies use deep Pacific $\delta^{13}\text{C}$ time series as a proxy for global mean $\delta^{13}\text{C}$ change (Shackleton et al., 1983; Curry and Oppo, 1997; Lisiecki et al., 2008). Given the large volume and carbon storage capacity of the deep Pacific, its $\delta^{13}\text{C}$ change should be similar in magnitude and timing to the mean ocean $\delta^{13}\text{C}$ change; however, no study has yet confirmed this relationship. For example, low sedimentation rates and poor carbonate preservation in the deep Pacific may limit how well deep Pacific $\delta^{13}\text{C}$ time series resolve changes in mean ocean $\delta^{13}\text{C}$. Additionally, large changes in Atlantic or Indian Ocean $\delta^{13}\text{C}$ could alter the timing of global mean $\delta^{13}\text{C}$ relative to the Pacific. By constructing a global benthic $\delta^{13}\text{C}$ stack, we can now directly compare deep Pacific $\delta^{13}\text{C}$ with global mean $\delta^{13}\text{C}$ change across the deglaciation.

2.3 Vertical gradients in benthic $\delta^{13}\text{C}$

25 A vertical gradient in the $\delta^{13}\text{C}$ of DIC between surface/intermediate waters and deep water results from a combination of physical, chemical, and biological processes. The air-sea gas exchange of CO_2 between the atmosphere and surface ocean generates a temperature-dependent fractionation (Lynch-Stieglitz et al., 1995). Biological productivity in the surface ocean preferentially incorporates ^{12}C into organic molecules, leaving ^{13}C -enriched DIC in surface waters. Conversely, deep water becomes depleted in ^{13}C due to remineralization of sinking organic carbon with a $\delta^{13}\text{C}$ signature of approximately -25‰. The accumulation of respired organic carbon in the deep ocean gradually increases deep water's DIC concentration while decreasing its $\delta^{13}\text{C}$ value. Thus, sinking organic carbon simultaneously creates vertical gradients in both $\delta^{13}\text{C}$ and DIC, creating low $\delta^{13}\text{C}$ and high DIC in the deep ocean and high $\delta^{13}\text{C}$ and low DIC in the surface ocean. However, deep water $\delta^{13}\text{C}$ is also affected by the transport of relatively high- $\delta^{13}\text{C}$ North Atlantic Deep Water into the deep Atlantic, where it mixes with low- $\delta^{13}\text{C}$ waters from the Southern Ocean (Talley, 2013).



Numerous $\delta^{13}\text{C}$ records from the well-characterized Atlantic Ocean demonstrate an enhanced vertical $\delta^{13}\text{C}$ gradient between intermediate and deep water during the LGM (*e.g.*, Curry and Lohmann (1982); Curry et al. (1988); Duplessy et al. (1988); Sarnthein et al. (1994); Hodell et al. (2003); Curry and Oppo (2005); Marchitto and Broecker (2006); Herguera et al. (2010)). The less well-sampled Pacific and Indian Oceans also show signs of enhanced stratification at the LGM based on stronger vertical $\delta^{13}\text{C}$ gradients and other nutrient and ventilation proxies (*e.g.*, Kallel et al. (1988); Matsumoto and Lynch-Stieglitz (1999); Matsumoto et al. (2002); Herguera et al. (2010); Lund et al. (2011b); Allen et al. (2015); Sikes et al. (2016)).

Multiple causes have been proposed for stronger vertical $\delta^{13}\text{C}$ gradients during the LGM, including increased surface productivity and export, increased ocean stratification, and changes in preformed $\delta^{13}\text{C}$ in regions of deep water formation (*e.g.*, Matsumoto et al. (2002); Curry and Oppo (2005); Marchitto and Broecker (2006); Lynch-Stieglitz et al. (2007); Marinov et al. (2008b, a); Herguera et al. (2010); Hesse et al. (2011); Lund et al. (2011a, b); Allen et al. (2015); Gebbie et al. (2015); Gloege et al. (2017); Menviel et al. (2017)). The large vertical $\delta^{13}\text{C}$ gradient at the LGM could indicate a strong biological pump and/or weak vertical mixing, either of which would increase deep ocean carbon storage. Although studies do not agree about the relative importance of different mechanisms in creating this vertical gradient, the consensus is that the enhanced vertical $\delta^{13}\text{C}$ gradient at the LGM is consistent with greater deep ocean carbon storage and that this carbon was transferred to the atmosphere and terrestrial biosphere during the glacial termination.

On orbital timescales, changes in the intermediate-to-deep vertical $\delta^{13}\text{C}$ gradient closely match atmospheric CO_2 , with weaker vertical $\delta^{13}\text{C}$ gradients corresponding to higher CO_2 levels (Oppo and Fairbanks, 1990; Flower et al., 2000; Hodell et al., 2003; Köhler et al., 2010; Lisiecki, 2010). This relationship supports the assertion that many of the processes affecting CO_2 also alter the vertical $\delta^{13}\text{C}$ gradient. Model simulations suggest that multiple processes contribute to deglacial pCO_2 rise (Bauska et al., 2016), including ocean temperature increase, enhanced Southern Ocean mixing rates (and the role of sea ice) (*e.g.*, Franois et al. (1997); Crosta and Shemesh (2002); Gildor et al. (2002); Hodell et al. (2003); Paillard and Parrenin (2004)), decreased alkalinity and carbon inventories (Yu et al., 2014; Kerr et al., 2017), reduced biological pump (Buchanan et al., 2016), enhanced global ocean circulation (Buchanan et al., 2016), and coral reef growth (*e.g.*, Vecsei and Berger (2004)). Here we evaluate the relationship between atmospheric CO_2 and vertical $\delta^{13}\text{C}$ change at millennial resolution across the deglaciation. It is beyond the scope of this study to evaluate how much of the change in CO_2 and the vertical $\delta^{13}\text{C}$ gradient at the LGM is associated with specific processes, such as changes in the biological pump (Archer et al., 2003; Köhler et al., 2005; Brovkin et al., 2007; Galbraith and Jaccard, 2015), deep water formation (McManus et al., 2004; Curry and Oppo, 2005) and/or Southern Ocean stratification (Lund et al., 2011b; Burke and Robinson, 2012).

3 Data

This study presents a compilation of 117 previously published benthic $\delta^{13}\text{C}$ time series of *Cibicides wuellerstorfi* in per mil relative to Vienna PeeDee Belemnite (V.P.D.B.) (Figure 1; Table A1). Each record in the compilation spans the time range 20-6 ka. Analysis does not extend after 6 ka because cores from several data-sparse regions were either too low-resolution or missing sediment from 6-0 ka. We only include $\delta^{13}\text{C}$ records with mean sample spacing better than 3 kyr (87% have a mean sample



spacing of less than 2 kyr). We excluded any records with sample gaps of 4 kyr or larger and excluded any cores affected by the phytodetritus effect ("Mackensen effect") as assessed by the original authors and the criteria from Peterson *et al.* (2014). We included one *C. kullenbergi* record from the deep South Atlantic (MD07-3076Q) (Waelbroeck *et al.*, 2011) which may record a more negative $\delta^{13}\text{C}$ value than *C. wuellerstorfi* at the LGM (Gottschalk *et al.*, 2016). Additionally, we use some cores with samples labeled "*C. spp*" that may include some *C. kullenbergi* (Table A1).

4 Methods

4.1 Stacking

Age models for cores were developed by aligning the benthic $\delta^{18}\text{O}$ records to the regional stacks of Stern and Lisiecki (2014), which have age models based on planktic foraminiferal ^{14}C ages. Because age model uncertainties are approximately 1-2 kyr (Stern and Lisiecki, 2014), and some of the $\delta^{13}\text{C}$ records analyzed have sample spacings of 2-3 kyr, our interpretation focuses on $\delta^{13}\text{C}$ features with timescales of about 2 kyr or greater. For example, we do not expect to reconstruct abrupt changes associated with the onset of the Bölling-Alleröd or with centennial-scale CO_2 changes (Marcott *et al.*, 2014). Because $\delta^{13}\text{C}$ record resolution varies between sites, we interpolate the $\delta^{13}\text{C}$ records to an even 1-kyr spacing, which introduces an additional source of uncertainty in the data. Although combining information from multiple records inherently risks distorting the true ocean state, this risk is counterbalanced by the potential for improved signal-to-noise when estimating regional and global signals. In supplemental material, we provide the original, uninterpolated records from all 117 sites, which could be used for comparison with transient deglacial ocean circulation experiments.

We define regions within ocean basins based on the spatial patterns in benthic $\delta^{13}\text{C}$, for example, differing LGM $\delta^{13}\text{C}$ values between intermediate and deep sites (Figure 2). In the North Atlantic, we separate the intermediate North Atlantic (INA, 0.5-2 km) from the upper deep North Atlantic (UDNA, 2-4 km) and the lower deep North Atlantic (LDNA, >4 km). Because the South Atlantic has fewer records than the North Atlantic (Table 1) and a different vertical $\delta^{13}\text{C}$ structure (Figure 2), we define the intermediate South Atlantic (ISA) as 0.5-2.5 km and the deep South Atlantic (DSA) as >2.5 km. We separate the Indo-Pacific into four regions: the intermediate Indian (II, 0.5-2 km), intermediate Pacific (IP, 0.5-2 km), deep Indian (DI, >2 km), and deep Pacific (DP, >2 km). The longitude boundaries between the Atlantic, Indian, and Pacific basins are the same as in Peterson *et al.* (2014). To create regional stacks, we average the interpolated $\delta^{13}\text{C}$ records in each region (Figure 2; Table A1). Most regions contain at least six cores; however, the intermediate and deep Indian regions each contain only two $\delta^{13}\text{C}$ records.

To calculate an intermediate, deep, and global mean $\delta^{13}\text{C}$ stacks (Figure 3, Figure 4), we calculated the volume of water in each region defined above (Table 1) and averaged the regional stacks using volume weighting as a percent of total volume (using a depth range of 0.5-5 km). Thus, we represent regions proportional to their volume rather than over-representing well-sampled regions. These global stacks include benthic $\delta^{13}\text{C}$ records from sites in the Atlantic, Indian, and Pacific Oceans but excludes the Southern Ocean, Arctic Ocean, and shallow inland seas. Additionally, this compilation only includes benthic $\delta^{13}\text{C}$ records from below 0.5 km; therefore, we refrain from interpreting or making assumptions about $\delta^{13}\text{C}$ above 0.5 km. Planktic



$\delta^{13}\text{C}$ data suggest that mixed layer $\delta^{13}\text{C}$ values may closely track atmospheric $\delta^{13}\text{C}$ change (Eggleston et al., 2016; Hertzberg et al., 2016).

We calculate a vertical $\delta^{13}\text{C}$ gradient ($\Delta\delta^{13}\text{C}_{I-D}$) using the volume-weighted intermediate and deep regional stacks from the Atlantic and Pacific. The Indian Ocean regional stacks are excluded from this vertical gradient calculation because each Indian region includes only two cores, making these regional stacks more susceptible to noise. A global vertical $\delta^{13}\text{C}$ gradient that includes the Atlantic, Indian, and Pacific Oceans (AIP $\Delta\delta^{13}\text{C}_{I-D}$) is provided in the supplemental materials (Figure A1, Table A2). Additionally, we construct a vertical $\delta^{13}\text{C}$ gradient between the intermediate North Atlantic and deep Pacific ($\Delta\delta^{13}\text{C}_{(INA/2)-DP}$) (Lisiecki, 2010) and compare both representations of the vertical $\delta^{13}\text{C}$ gradient to atmospheric CO_2 .

We estimate stack uncertainty using Monte Carlo simulations that account for the effects of measurement uncertainty and intra-region $\delta^{13}\text{C}$ variability. Specifically, we generate 95% confidence intervals for the stacks using 10,000 bootstrapped iterations that randomly resample $\delta^{13}\text{C}$ records from each region. During the resampling process, we also simulate measurement uncertainty in each record by adding Gaussian white noise with a standard deviation of 0.15‰ (Gebbie et al., 2015). Differences in the benthic $\delta^{13}\text{C}$ stack between different Monte Carlo simulations, each with 10,000 iterations, is on the order of 0.02‰ at the LGM (20-19 ka) and even smaller for the Holocene (6 ka). It is beyond the scope of the current study to quantify uncertainty associated with portions of the ocean for which there is no available data.

4.2 Comparison to CO_2

To compare the $\delta^{13}\text{C}$ data to atmospheric CO_2 changes from 20-6 ka, we spliced together the atmospheric CO_2 records of Marcott et al. (2014) and Monnin et al. (2004). No correction was necessary to splice these records at 8.9860 ka because the CO_2 value of 265.45 p.p.m.v. at 8.9855 ka in Monnin et al. (2004) agrees well with the value of 265.2 p.p.m.v. at 8.9730 ka in Marcott et al. (2014) (Figure 5). For quantitative comparison, we down-sampled the spliced CO_2 record by interpolating it to the same 1-kyr resolution of our benthic $\delta^{13}\text{C}$ stacks.

Additionally, we examine the potential for differences in the timing of CO_2 and $\delta^{13}\text{C}$ change that could be caused by lags in the climate system or age model uncertainty. We calculate correlation coefficients for different potential lags by interpolating the spliced CO_2 record with different time offsets, using lags that range from +1000 yr to -1000 yr in increments of 100 yr. For example, a 100-yr lag in CO_2 relative to the vertical $\delta^{13}\text{C}$ gradient would be represented by comparing $\delta^{13}\text{C}$ values at 6, 7, ... 20 ka with CO_2 values at 5.9, 6.9, ..., and 19.9 ka. Conversely, a CO_2 lead of 100 yr would be suggested if the correlation between the two is maximized for CO_2 values at 6.1, 7.1, ..., 20.1 ka.

Testing the significance of correlations between $\delta^{13}\text{C}$ and CO_2 is complicated by the fact that both time series are autocorrelated, *i.e.*, each data point is highly correlated with the value immediately before or after. To reduce the impact of autocorrelation, we pre-whiten the data by taking the difference between successive 1-kyr samples before calculating the linear correlation and its statistical significance. Our assessment of the statistical significance of the correlations accounts for the reduction in the number of degrees of freedom in the data associated with pre-whitening and/or allowing time lags between $\delta^{13}\text{C}$ and CO_2 observations.



5 Results

5.1 Comparison to LGM and Holocene reconstructions

Although our time series compilation has fewer core sites than some previous studies of LGM $\delta^{13}\text{C}$, it preserves the large-scale features of these LGM $\delta^{13}\text{C}$ reconstructions, such as enhanced vertical and meridional Atlantic $\delta^{13}\text{C}$ gradients (Figure 2) (*e.g.*,
5 Curry and Oppo (2005); Peterson et al. (2014)). Vertical $\delta^{13}\text{C}$ gradients are strongest in the glacial North Atlantic, closely followed by the glacial South Atlantic (Peterson et al., 2014). Indo-Pacific $\delta^{13}\text{C}$ values are more depleted than North Atlantic $\delta^{13}\text{C}$ values of the same depth. The most depleted $\delta^{13}\text{C}$ values in the compilation are from the high-latitude deep South Atlantic during the LGM, possibly due to inclusion of data from *C. kullenbergi* (Gottschalk et al., 2016). Equatorial deep South Atlantic records at the LGM have $\delta^{13}\text{C}$ values similar to equatorial deep Indo-Pacific $\delta^{13}\text{C}$ records. However, our compilation lacks
10 Indo-Pacific sites deeper than 3.5 km.

At 6 ka the $\delta^{13}\text{C}$ values in this compilation generally resemble the Holocene compilation of Peterson et al. (2014). Minor differences could result from Peterson *et al.* (2014) using Holocene data from 6-0 ka and including more North Pacific sites and more sites from 0.5-1.5 km depth.

5.2 Regional stacks

15 We create nine regional $\delta^{13}\text{C}$ stacks from 20-6 ka (Figure 3, Table 1). Six of the regional $\delta^{13}\text{C}$ stacks increase steadily from approximately 20-18 ka to 6 ka (LDNA, DSA, II, IP, DI, DP). Small deviations in the trend of the Indian $\delta^{13}\text{C}$ stacks are interpreted as noise because these stacks each contain only two cores. Three Atlantic regions (INA, ISA, UDNA) show a decrease in $\delta^{13}\text{C}$ from approximately 19-15 ka and then an increase from 14-6 ka, as described in previous studies (*e.g.*, Hodell et al. (2008); Thornalley et al. (2010); Hodell et al. (2010); Lund et al. (2011a); Tessin and Lund (2013); Oppo et al. (2015)).
20 The UDNA $\delta^{13}\text{C}$ stack is briefly similar to the LDNA at 16 ka and then resembles the ISA stack from 14-6 ka. The DI and DSA $\delta^{13}\text{C}$ values are generally similar across the deglaciation except that the DSA $\delta^{13}\text{C}$ begins increasing at 18 ka while the DI $\delta^{13}\text{C}$ increase begins at 16 ka. The intermediate-depth $\delta^{13}\text{C}$ stacks in the Indian and Pacific Oceans are very similar for most of the time interval.

Across the deglaciation, the vertical $\delta^{13}\text{C}$ gradient weakens in the Atlantic, most noticeably in the North Atlantic (INA-
25 LDNA: 1.20‰ at 20 ka and 0.31‰ at 6 ka). Vertical gradients in the Indian and Pacific Oceans show much less change. The largest spread in $\delta^{13}\text{C}$ values is observed from 20-18 ka, when the intermediate North Atlantic and deep South Atlantic regions differ by 1.6‰; this gradient has decreases to 0.47‰ at 11-10 ka. The maximum difference between regions at 6 ka is 0.91‰ between the intermediate North Atlantic (most enriched) and the deep Indian (most depleted).

5.3 Volume-weighted stacks and global mean $\delta^{13}\text{C}$ stack

30 A global mean $\delta^{13}\text{C}$ stack is constructed by volume weighting all nine regional stacks. However, we construct two different versions of the intermediate and deep $\delta^{13}\text{C}$ stacks, with and without the Indian stacks, because the Indian regions each contain



only two records. Both versions of the intermediate and deep stacks show similar trends, but we focus our analysis on the version that uses only the Atlantic and Pacific regions, which should be less susceptible to noise (Figure 4, Table 1). Results for the intermediate and deep $\delta^{13}\text{C}$ stacks that include Indian Ocean are provided in supplemental materials (Figure A1, Table A2). The volume-weighted intermediate, deep, and global mean $\delta^{13}\text{C}$ stacks increase across the deglaciation, but the magnitude of change is larger for the deep $\delta^{13}\text{C}$ stack (0.46‰) than the intermediate $\delta^{13}\text{C}$ stack (0.24‰) (Table 1, Figure 4). We define the vertical $\delta^{13}\text{C}$ gradient, $\Delta\delta^{13}\text{C}_{I-D}$, as the difference between the volume-weighted Atlantic and Pacific intermediate and deep stacks. This gradient is largest at 20 ka (0.40‰) and shrinks to 0.24‰ by 6 ka.

The volume-weighted global $\delta^{13}\text{C}$ stack holds nearly steady from 20 to 19 ka at approximately 0.00‰ (95% CI: -0.10 to 0.09‰ at 19 ka) and then increases from 18-6 ka, reaching a value of 0.37‰ (95% CI: 0.26 to 0.49‰) at 6 ka. The change from 20 to 6 ka in the global stack is 0.36‰ (95% CI: 0.25 to 0.46‰), which agrees to within uncertainty with the LGM-to-Holocene mean $\delta^{13}\text{C}$ change estimate of 0.38‰ (95% CI: 0.30 to 0.46‰) for 0.5-5 km from (Peterson et al., 2014). Recall that the mean $\delta^{13}\text{C}$ estimate from our global stack is not quite a whole-ocean $\delta^{13}\text{C}$ estimate because we do not include data from the surface (<0.5 km), Southern Ocean (>65S), or bottom waters (>5 km). Estimates of whole-ocean $\delta^{13}\text{C}$ change are slightly smaller at 0.34‰ (95% CI: 0.15 to 0.53‰) (Peterson et al., 2014) and 0.32‰ (95% CI: 0.12 to 0.52‰) (Gebbie et al., 2015). The surface ocean (0-0.5 km) has enriched $\delta^{13}\text{C}$ values with much less deglacial change (Eggleston et al., 2016; Hertzberg et al., 2016).

6 Discussion

6.1 Terrestrial carbon storage and global mean benthic $\delta^{13}\text{C}$

The long-standing explanation for mean benthic $\delta^{13}\text{C}$ change across the deglaciation is an increase in the size of the terrestrial biosphere (Shackleton, 1977; Curry et al., 1988; Duplessy et al., 1988). Here we compare the timing of changes in our global mean $\delta^{13}\text{C}$ stack (*i.e.*, a monotonic increase from 19-6 ka, Figure 4B) with model simulations and other terrestrial biosphere reconstructions.

A carbon isotope-enabled transient model from LPJ-DVGM simulated a mean ocean $\delta^{13}\text{C}$ increase beginning at 21 ka, with the most rapid changes occurring from 17-10.5 ka (Kaplan et al., 2002). In these experiments, the terrestrial biosphere began expanding around 18-16.5 ka (Joos et al., 2004; Köhler et al., 2005) and rapidly increased from 17-9 ka, with 70% of terrestrial carbon storage change occurring before the Holocene (11.5 ka) (Kaplan et al., 2002). In our global $\delta^{13}\text{C}$ stack, 67% of the $\delta^{13}\text{C}$ change occurs between 19-11 ka while the remaining 33% of $\delta^{13}\text{C}$ change occurs from 11-6 ka.

Simulations from HadCM3 estimated that 45-70% of terrestrial biosphere expansion occurred between 18-14 ka (Davies-Barnard et al., 2017). Dramatically different trends were observed from 14-6 ka in simulations with different assumptions about carbon storage under glacial ice sheets and on continental shelves. The simulation that most closely resembles our global mean $\delta^{13}\text{C}$ stack is the simulation that releases carbon from under ice sheets to the atmosphere and does not accumulate carbon on exposed continental shelves (Figure 5). This simulation is also the only one which agrees with terrestrial carbon storage change estimates of 440 PgC based on whole-ocean mean $\delta^{13}\text{C}$ change (*e.g.*, Peterson et al., 2014).



Climate model simulations of the Holocene using a global pollen synthesis, the biomization method, and vegetation models (HadCM3, FAMOUS, and BIOME4) suggest that the global average area for most carbon-rich megabiomes (i.e., excluding grasslands and dry shrubland) increased from 10-2 ka and net primary productivity increased from 8-2 ka (Hoogakker et al., 2016). This is consistent with our observation that the global mean benthic $\delta^{13}\text{C}$ trend continued until at least 6 ka. Dramatic
5 land use changes from agricultural practices, another potential mechanism for terrestrial carbon change, did not begin until 4.5 ka (Ruddiman and Ellis, 2009). More detailed evaluation of Holocene terrestrial carbon storage changes will require improved spatial coverage for $\delta^{13}\text{C}$ records from 6-0 ka.

6.2 Global mean $\delta^{13}\text{C}$ and deep Pacific $\delta^{13}\text{C}$

Previous studies have assumed deep Pacific $\delta^{13}\text{C}$ can be used as a proxy for global mean $\delta^{13}\text{C}$ because the deep Pacific
10 constitutes about 30% of the ocean volume and is not strongly affected by shifting water mass boundaries (e.g., Shackleton et al. (1983); Curry and Oppo (1997); Lisiecki et al. (2008)). From 20-6 ka, the global mean and deep Pacific $\delta^{13}\text{C}$ stacks show similar patterns of change (Figure 6) and fall along a tight regression line

$$\delta^{13}\text{C}_{global} = 1.02 \pm 0.06\% \times \delta^{13}\text{C}_{DP} + 0.18 \pm 0.01\% \text{‰}$$

The two time series are highly correlated ($r^2=0.99$), which is not surprising because the large volume of the deep Pacific exerts
15 a strong influence on the global mean $\delta^{13}\text{C}$ stack. However, when the stacks are pre-whitened to account for autocorrelation, their correlation falls on the edge of statistical significance ($p=0.05$). The statistical significance of this correlation is likely limited by the relatively short time interval analyzed and/or noise in the deep Pacific stack, which contains only seven $\delta^{13}\text{C}$ records.

A carbon cycle box model simulated a strong correlation between deep Pacific $\delta^{13}\text{C}$ and CO_2 across several glacial cycles
20 ($r^2=0.96$) (Köhler et al., 2010). The correlation between our deep Pacific $\delta^{13}\text{C}$ stack and CO_2 is statistically significant after pre-whitening ($r^2=0.62$, $p=0.01$), but global mean $\delta^{13}\text{C}$ and CO_2 are not ($r^2=0.20$, $p=0.24$). Our compilation of Pacific records is likely insufficient to determine whether deep Pacific $\delta^{13}\text{C}$ correlates better with global mean $\delta^{13}\text{C}$ or atmospheric CO_2 . This issue could be better resolved using a $\delta^{13}\text{C}$ compilation spanning multiple glacial cycles and including more deep Pacific sites.

6.3 Vertical $\delta^{13}\text{C}$ gradient and atmospheric CO_2

The vertical $\delta^{13}\text{C}$ gradient ($\Delta\delta^{13}\text{C}_{I-D}$) in our compilation resembles the inverse of CO_2 change across the deglaciation (Figure
7), as would be expected if they are both strongly influenced by changes in deep ocean carbon storage (Flower et al., 2000; Oppo and Horowitz, 2000; Hodell et al., 2003). Alternatively, one orbital-scale study found a stronger correlation with CO_2 using the gradient between the deep Pacific and half the INA $\delta^{13}\text{C}$ stack ($\Delta\delta^{13}\text{C}_{(INA/2)-DP}$) Lisiecki (2010). Both vertical
25 $\delta^{13}\text{C}$ gradients ($\Delta\delta^{13}\text{C}_{I-D}$ and $\Delta\delta^{13}\text{C}_{(INA/2)-DP}$) decrease from 18-11 ka over the same time interval that atmospheric
30 CO_2 increases. In contrast, the global mean $\delta^{13}\text{C}$ stack increases at a relatively steady pace from 19-6 ka. Thus, the vertical $\delta^{13}\text{C}$ gradient records a distinctly different signal than the global mean $\delta^{13}\text{C}$.

The vertical $\delta^{13}\text{C}$ gradients decrease most rapidly across two time steps, 18-17 ka and 12-11 ka. The first change at 18 ka is approximately synchronous with the start of atmospheric CO_2 rise (Marcott et al., 2014) and a decrease of 0.3‰ in the $\delta^{13}\text{C}$



of atmospheric CO₂ (Eggleston et al., 2016). In the Southern Ocean at 18 ka, proxy records indicate a decrease in aeolian dust deposition accompanied by lower marine productivity (Martínez-García et al., 2009) and a decrease in winter sea ice cover, which likely reduced vertical stratification (Ferrari et al., 2014). The second rapid change in the vertical $\delta^{13}\text{C}$ gradients at 12 ka approximately coincides with rapidly increasing atmospheric CO₂ from 13-11.5 ka and a decrease of 0.1‰ in the $\delta^{13}\text{C}$ of atmospheric CO₂.

From 11 to 6 ka, atmospheric CO₂ remains nearly constant with a small (approximately 10 ppm) decrease from 11-8 ka. The vertical $\delta^{13}\text{C}$ gradients are also relatively steady from 11-6 ka, with a slight increase in both gradients from 9-8 ka. The small decrease in atmospheric CO₂ beginning at 11 ka (Marcott et al., 2014) has been variously attributed to growth of the terrestrial biosphere, sea level rise, and an increase in gas exchange through reduced sea ice cover (Kaplan et al., 2002; Joos et al., 2004; Köhler and Fischer, 2004; Köhler et al., 2005, 2010).

Although CO₂ correlates strongly with both $\Delta\delta^{13}\text{C}_{I-D}$ ($r^2=-0.98$) and $\Delta\delta^{13}\text{C}_{(INA/2)-DP}$ ($r^2=-0.98$), we must pre-whiten these time series to remove autocorrelation before assessing the statistical significance of their correlation. At the 95% confidence level, atmospheric CO₂ significantly correlates with both $\Delta\delta^{13}\text{C}_{I-D}$ ($r^2=-0.70$; $p<0.01$) and $\Delta\delta^{13}\text{C}_{(INA/2)-DP}$ ($r^2=-0.79$; $p<0.01$) (Figure A1, Table 2). Better correlation with $\Delta\delta^{13}\text{C}_{(INA/2)-DP}$ could be because of better age control and higher resolution $\delta^{13}\text{C}$ records in the INA region than the other intermediate regions. Determining whether the $\Delta\delta^{13}\text{C}_{(INA/2)-DP}$ gradient or the volume-weighted vertical $\delta^{13}\text{C}$ gradient correlates better with atmospheric CO₂ will require data with better spatial coverage and/or a longer time span.

Because our comparison of the vertical $\delta^{13}\text{C}$ gradient and CO₂ could be affected by differences in timing caused by carbon cycle processes or age model uncertainty, we additionally investigate whether the correlations between CO₂ and the vertical $\delta^{13}\text{C}$ gradient would be improved by age model shifts (Table 2). The correlation between CO₂ is maximized when $\Delta\delta^{13}\text{C}_{I-D}$ lags CO₂ by 300 years or when $\Delta\delta^{13}\text{C}_{(INA/2)-DP}$ leads CO₂ by 200 years (Table 2), both of which are within the age uncertainty of the sediment core age models. Thus, changes in atmospheric CO₂ and vertical $\delta^{13}\text{C}$ gradients appear synchronous to within age model uncertainty.

The prevailing processes that potentially explain atmospheric CO₂ change during glacial cycles include the efficiency of the biological pump (Martínez-García et al., 2009; Galbraith and Jaccard, 2015), circulation changes (Ferrari et al., 2014; Lacerra et al., 2017; Menviel et al., 2017; Sikes et al., 2017; Wagner and Hendy, 2017), or a combination of these and/or other processes (Bauska et al., 2016; Skinner et al., 2017). These processes could influence the carbon cycle on different timescales (Bauska et al., 2016; Kohfeld and Chase, 2017) and/or in different regions (*e.g.*, (Gu et al., 2017)), which could confound interpretations of which processes are responsible for atmospheric CO₂ change. However, because both productivity and circulation change would affect the vertical $\delta^{13}\text{C}$ gradient while changing atmospheric CO₂, we interpret our results as supporting the importance of the deep ocean as a reservoir for storing glacial carbon from either or both processes. Furthermore, these results support the use of vertical $\delta^{13}\text{C}$ gradients as a proxy for glacial-interglacial CO₂ change (Lisiecki, 2010).



7 Conclusions

We present regional $\delta^{13}\text{C}$ stacks and volume-weighted intermediate, deep, and global mean $\delta^{13}\text{C}$ stack from a compilation of 117 benthic *C. wuellerstorfi* $\delta^{13}\text{C}$ records, which span 20 to 6 kyr with a mean age resolution better than 2 kyr. Age models are based on $\delta^{18}\text{O}$ alignments to regional stacks with radiocarbon dating, with age model uncertainties for each core of approximately 1-2 kyr. The volume-weighted mean $\delta^{13}\text{C}$ change estimate of 0.36‰ (95% CI: 0.25 to 0.46‰) from the 117 cores in this study is similar to the estimate of Peterson *et al.* (2014) based on 480 cores. This compilation also shows spatial patterns of benthic $\delta^{13}\text{C}$ that are similar to higher resolution reconstructions of the Holocene and Last Glacial Maximum time slices.

The global mean $\delta^{13}\text{C}$ stack is interpreted as recording an increase in the size of the terrestrial biosphere from 19 to 6 ka, in agreement with modeling studies (Kaplan *et al.*, 2002; Joos *et al.*, 2004). To constrain the timing of the end of terrestrial biosphere expansion, future work should focus on extending this estimate through the Late Holocene. Furthermore, the $\delta^{13}\text{C}$ changes from 20 ka to 6 ka suggest that a deep Pacific $\delta^{13}\text{C}$ stack can be used as a proxy for global mean $\delta^{13}\text{C}$ with an offset of 0.18‰. Future work should aim to validate this result over one or more glacial cycles and using more deep Pacific records. Both vertical $\delta^{13}\text{C}$ gradients, between intermediate and deep water ($\Delta\delta^{13}\text{C}_{I-D}$) and intermediate North Atlantic and deep Pacific ($\Delta\delta^{13}\text{C}_{(INA/2)-DP}$), are interpreted as proxies for changes in deep ocean carbon storage. We find that millennial-scale features in $\Delta\delta^{13}\text{C}_{I-D}$ and $\Delta\delta^{13}\text{C}_{(INA/2)-DP}$ are significantly correlated with atmospheric CO_2 changes from 20-6 ka. Based on these comparisons, we conclude that the four-dimensional compilation of globally distributed $\delta^{13}\text{C}$ time series presented here provides useful constraints for global carbon cycle reconstructions and for comparison with deglacial simulations from isotope-enabled Earth systems models.

20 *Data availability.* The original data and publication citations along with this data synthesis are made available in supplemental files.

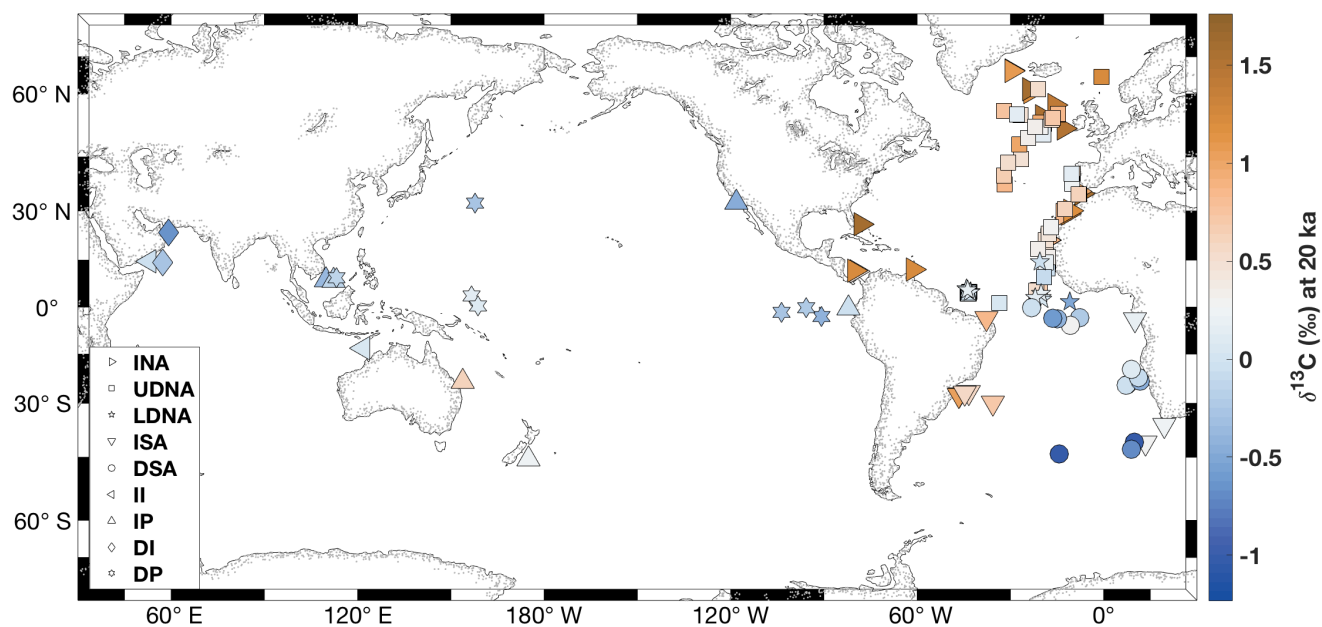


Figure 1. Locations of 117 core sites compiled for this study, color coded by LGM $\delta^{13}\text{C}$ estimates at each core site. Markers indicate locations of cores in the nine regions: INA = intermediate North Atlantic; UDNA = upper deep North Atlantic; LDNA = lower deep North Atlantic; ISA = intermediate South Atlantic; DSA = deep South Atlantic; II = intermediate Indian; DI = deep Indian; IP = intermediate Pacific; DP = deep Pacific.

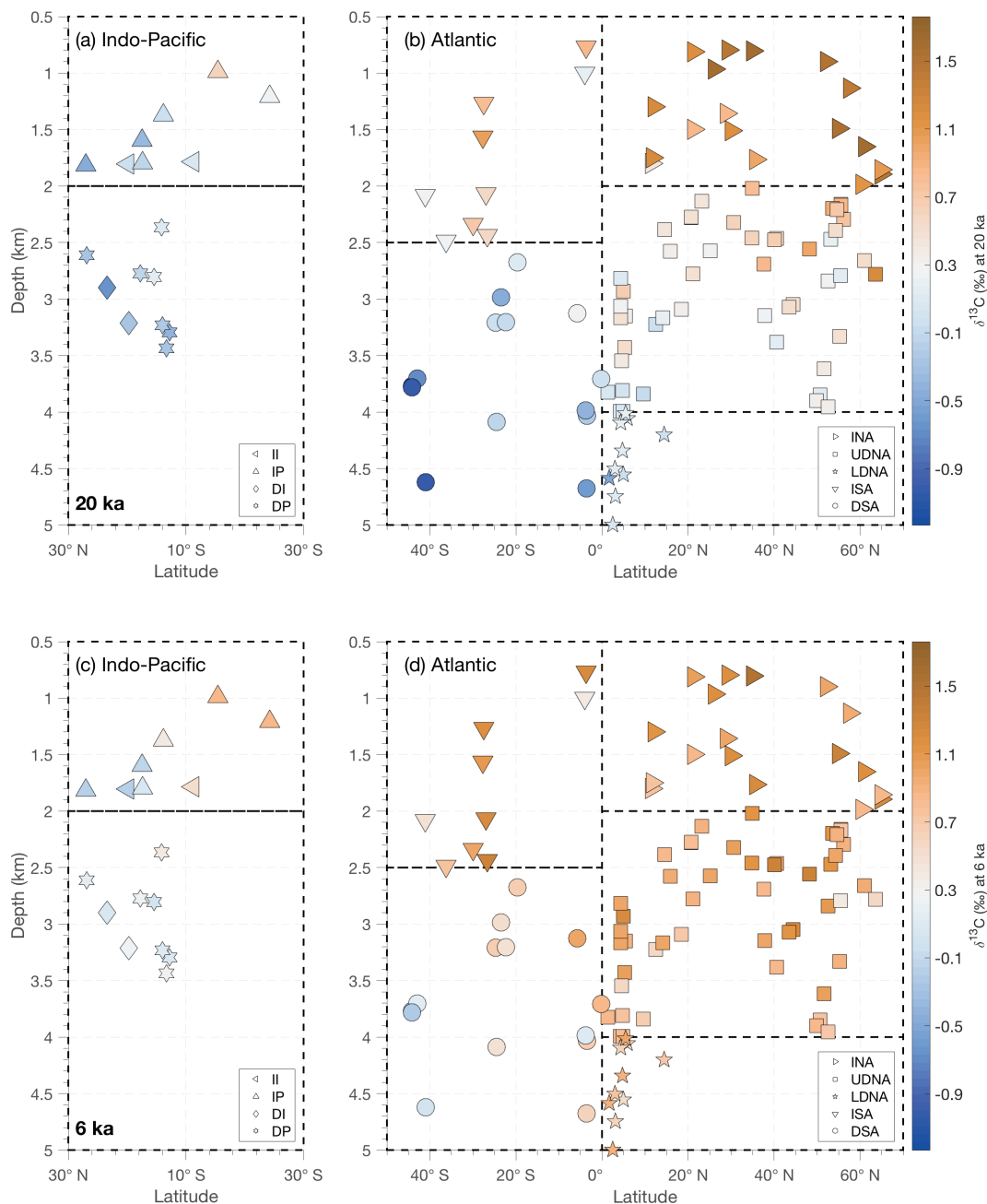


Figure 2. The three-dimensional structure of $\delta^{13}\text{C}$ in Indian and Pacific Oceans (a and c) and Atlantic (b and d) shown as zonally collapsed cross sections (latitude vs. depth) with the same marker scheme as in Figure 1. Dotted lines indicate region boundaries. Colors show the $\delta^{13}\text{C}$ value at each site for the LGM (20 ka, top row) and Holocene (6 ka, bottom row). Note that latitudes on the x-axis are oriented so the Southern Ocean is in the center of the figure. Additional time slices (in 1-kyr intervals from 20-6 ka) and an animation of deglacial $\delta^{13}\text{C}$ changes can be found in the supplemental materials.

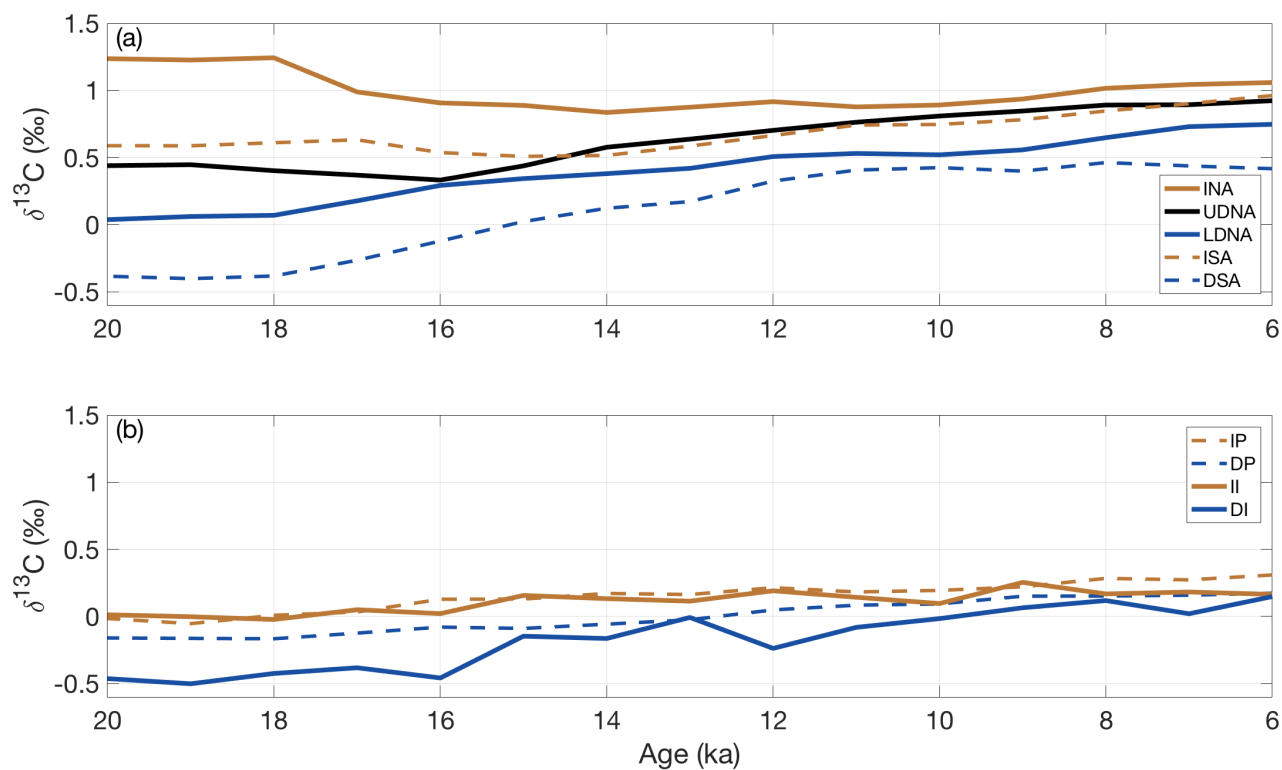


Figure 3. Regional stacks for the (a) Atlantic and (b) Indian and Pacific Oceans. Note the x- and y-axes are identically scaled. INA = intermediate North Atlantic; UDNA = upper deep North Atlantic; LDNA = lower deep North Atlantic; ISA = intermediate South Atlantic; DSA = deep South Atlantic; II = intermediate Indian; DI = deep Indian; IP = intermediate Pacific; DP = deep Pacific.

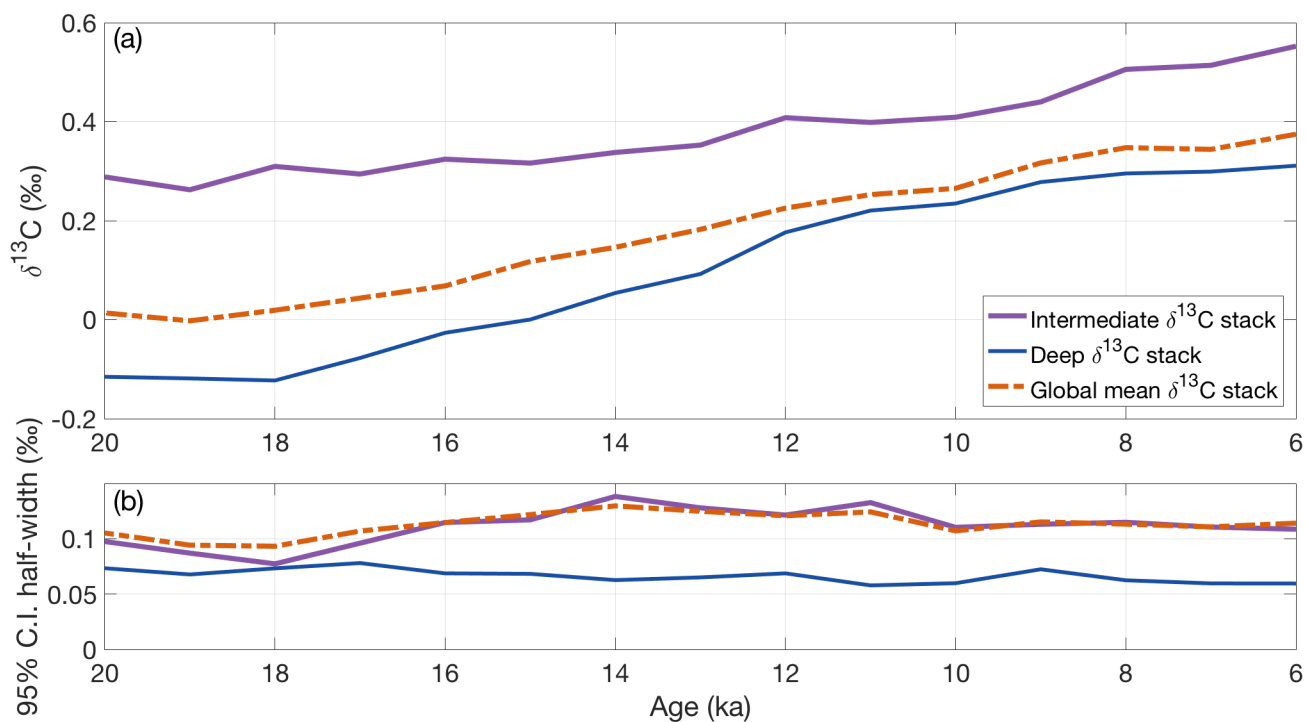


Figure 4. Volume-weighted stacks. (a) The volume-weighted global stack is calculated based on all nine regional stacks. However, the intermediate and deep stacks shown here only include Atlantic and Pacific data due to the small amount of Indian data. A comparison of these stacks with ones which include the Indian stacks is provided in Figure A1. (b) 95% confidence interval half-width showing the change in uncertainty across the deglaciation for each stack.

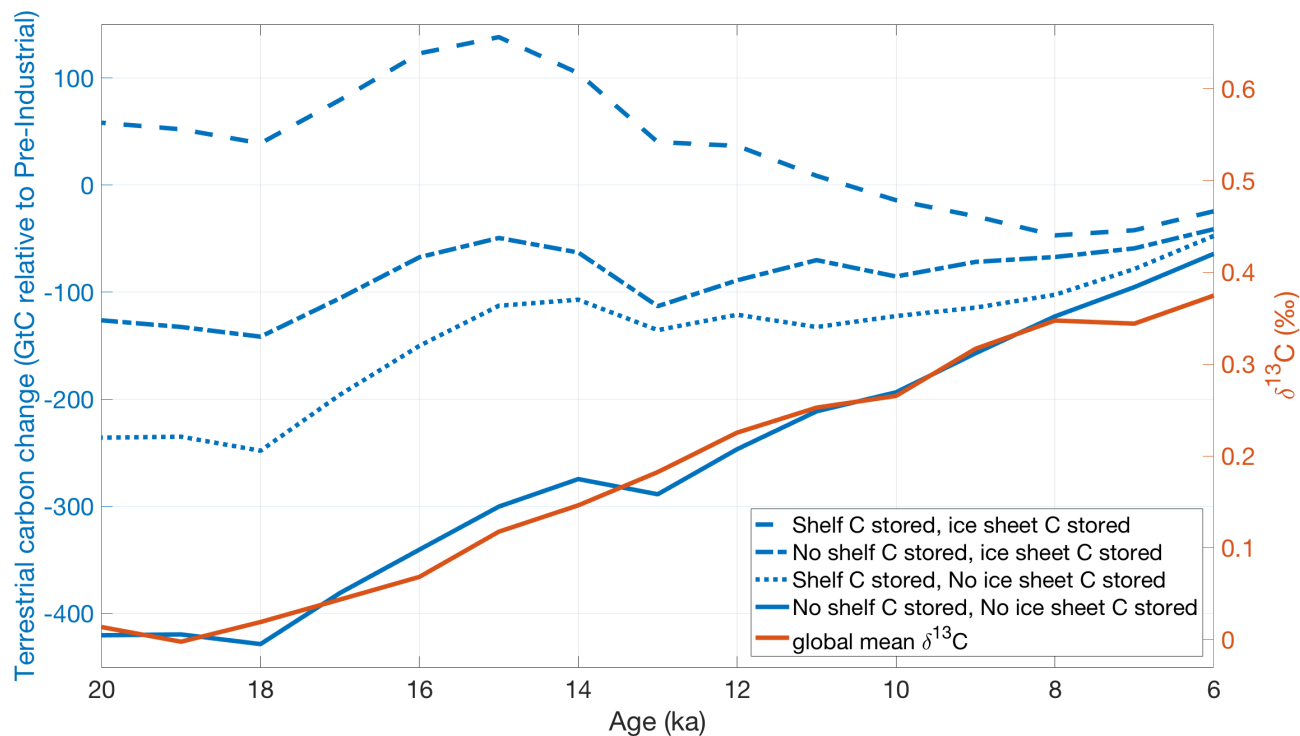


Figure 5. Time series of various HadCM3 simulations of terrestrial carbon storage (biosphere and soils) anomalies relative to the pre-Industrial plotted in blue (Davies-Barnard et al., 2017) and our global mean $\delta^{13}\text{C}$ approximation of terrestrial carbon storage plotted in orange. Global mean $\delta^{13}\text{C}$ change closely resembles one simulation (solid blue) that releases carbon from under ice sheets to the atmosphere and does not store carbon on continental shelves.

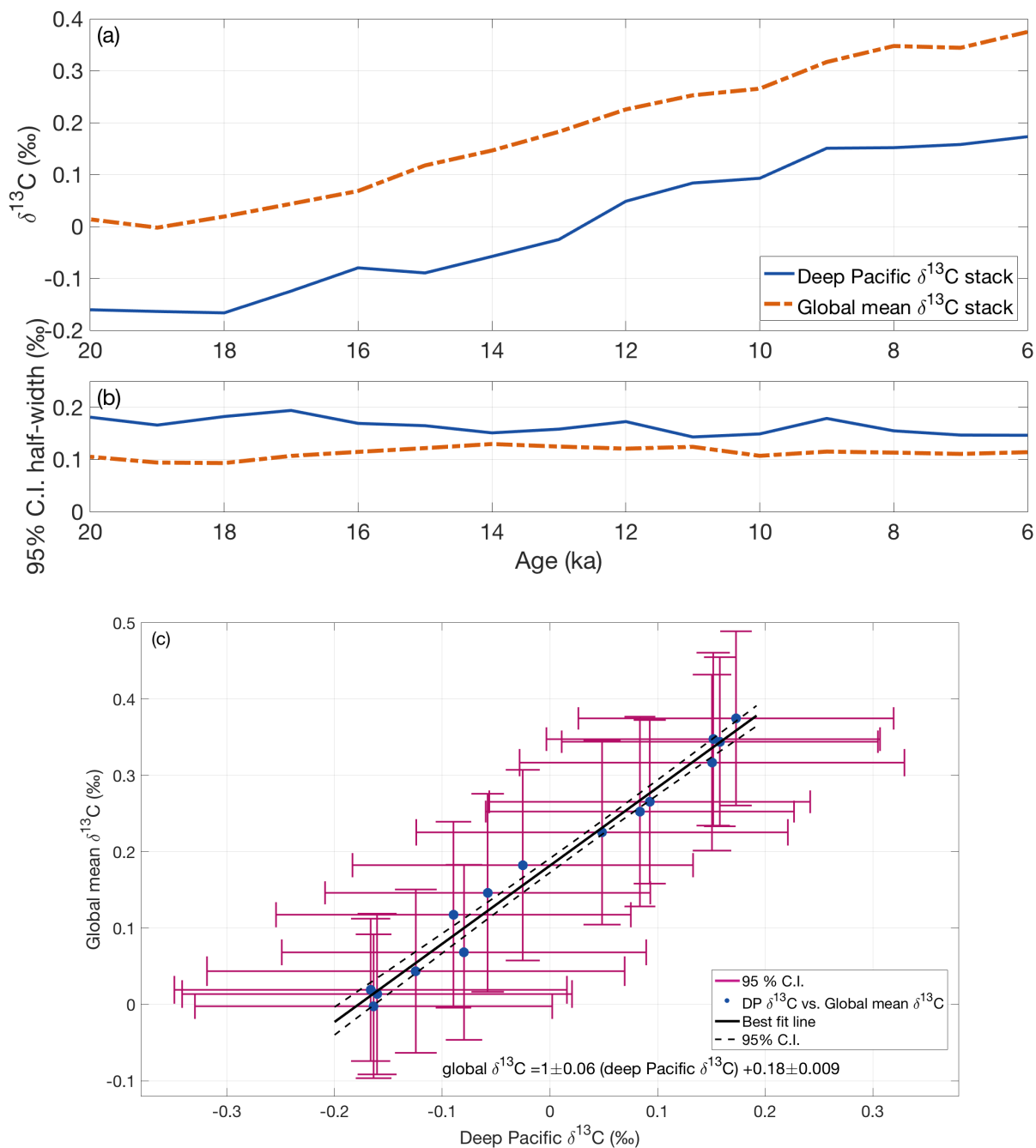


Figure 6. (a) Time series of global mean ocean $\delta^{13}\text{C}$ stack and deep Pacific $\delta^{13}\text{C}$ stacks. (b) Half-width 95% confidence intervals for the global mean stack and deep Pacific stack. (c) Deep Pacific $\delta^{13}\text{C}$ stack vs. global mean $\delta^{13}\text{C}$ stack. Each point is the $\delta^{13}\text{C}$ value for one time slice with 95% confidence intervals (vertical and horizontal error bars). Time across the deglaciation progresses toward the upper right corner. The best-fit line for the two stacks is plotted as a solid line with 95% confidence interval dashed lines.

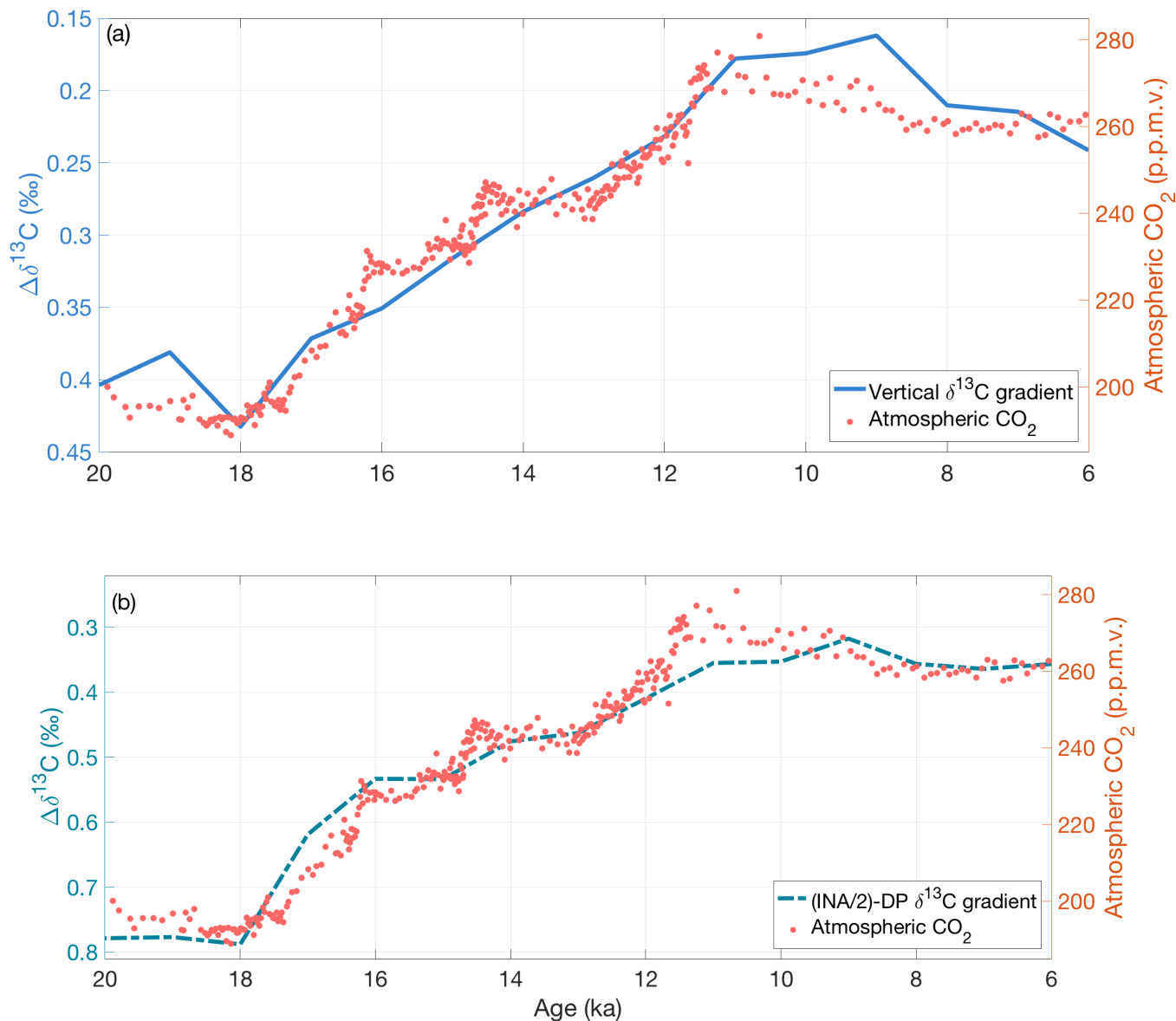


Figure 7. Comparison of atmospheric CO₂ with both AP vertical $\delta^{13}\text{C}$ gradient (a) and $\Delta\delta^{13}\text{C}_{(INA/2)-DP}$ gradient (b). Both vertical gradients closely resemble the spliced atmospheric CO₂ records (red circles) (Marcott et al., 2014; Monnin et al., 2004), but the $\Delta\delta^{13}\text{C}_{(INA/2)-DP}$ gradient is better correlated with atmospheric CO₂ from 20-6 ka. Recall the $\Delta\delta^{13}\text{C}_{(INA/2)-DP}$ gradient is not volume-weighted while the vertical AP $\delta^{13}\text{C}$ gradient is volume-weighted, hence the right y-axes between the top and bottom panels are not directly comparable.



Table 1. Region details: number of sites included, the regional volume as a percent of the core depth range (0.5-5 km, excluding shallow inland seas, Southern Ocean, and Arctic Ocean), and the mean $\delta^{13}\text{C}$ estimates at the LGM (20 ka), Holocene (6 ka), and the Holocene $\delta^{13}\text{C}$ minus LGM $\delta^{13}\text{C}$ difference. In parenthesis are bootstrapped mean $\delta^{13}\text{C}$ values and 95% confidence interval for the global mean $\delta^{13}\text{C}$.

Region name	Sites in stack	%Volume*	$\delta^{13}\text{C}_{Hol}(\text{‰})$	$\delta^{13}\text{C}_{LGM}(\text{‰})$	$\Delta\delta^{13}\text{C}_{Hol-LGM}(\text{‰})$
INA	18	5.0	1.06	1.24	-0.18
ISA	9	7.9	0.96	0.59	0.37
II	2	8.0	0.16	0.01	0.15
IP	6	24.3	0.31	-0.02	0.32
Intermediate _{w,m}	35	45.2	0.55	0.29	0.26
UDNA	49	5.4	0.92	0.44	0.48
LDNA	10	1.5	0.75	0.04	0.71
DSA	14	6.2	0.42	-0.38	0.80
DI	2	9.5	0.15	-0.46	0.61
DP	7	32.2	0.17	-0.16	0.33
Deep _{w,m}	82	54.8	0.31	-0.12	0.43
Global _{w,+}	117	77.7*	0.37	0.01	0.36 (95% CI: 0.25 to 0.46)

*Volume of core depth range (0.5-5 km) as a proportion of global volume

_w Volume-weighted $\delta^{13}\text{C}$ values

_m Excluding the Indian Ocean regions

₊ Atlantic, Indian, and Pacific Ocean regions



Table 2. Correlation coefficients and p-values between pre-whitened records. We pre-whitened to account for autocorrelated time series and calculated p-values to account for reduced degrees of freedom for pre-whitened and/or time lagged correlations. To investigate possible leads/lags between records, we shift the atmospheric CO₂ record in 100-year increments relative to the $\delta^{13}\text{C}$ stacks. The atmospheric CO₂ record is spliced from CO₂ records from Monnin et al. (2004) at 8.9855 ka and Marcott et al. (2014) at 8.9730 ka.

Record 1	Record 2	CO ₂ time shift (years)	Pre-whitened r ²	Pre-whitened p-value
Global mean $\delta^{13}\text{C}$ stack	Deep Pacific $\delta^{13}\text{C}$ stack	0	0.46	0.05
CO ₂	Deep Pacific $\delta^{13}\text{C}$ stack	0	0.62	0.008
CO ₂	Global $\delta^{13}\text{C}$ stack	0	0.20	0.24
CO ₂	Global $\delta^{13}\text{C}$ stack	-500	0.35	0.12
CO ₂	$\Delta\delta^{13}\text{C}_{I-D}$	0	-0.70	0.002
CO ₂	$\Delta\delta^{13}\text{C}_{I-D}$	+300	-0.73	0.002
CO ₂	$\Delta\delta^{13}\text{C}_{(INA/2)-DP}$	0	-0.79	0.0002
CO ₂	$\Delta\delta^{13}\text{C}_{(INA/2)-DP}$	-200	-0.82	0.0002



Appendix A

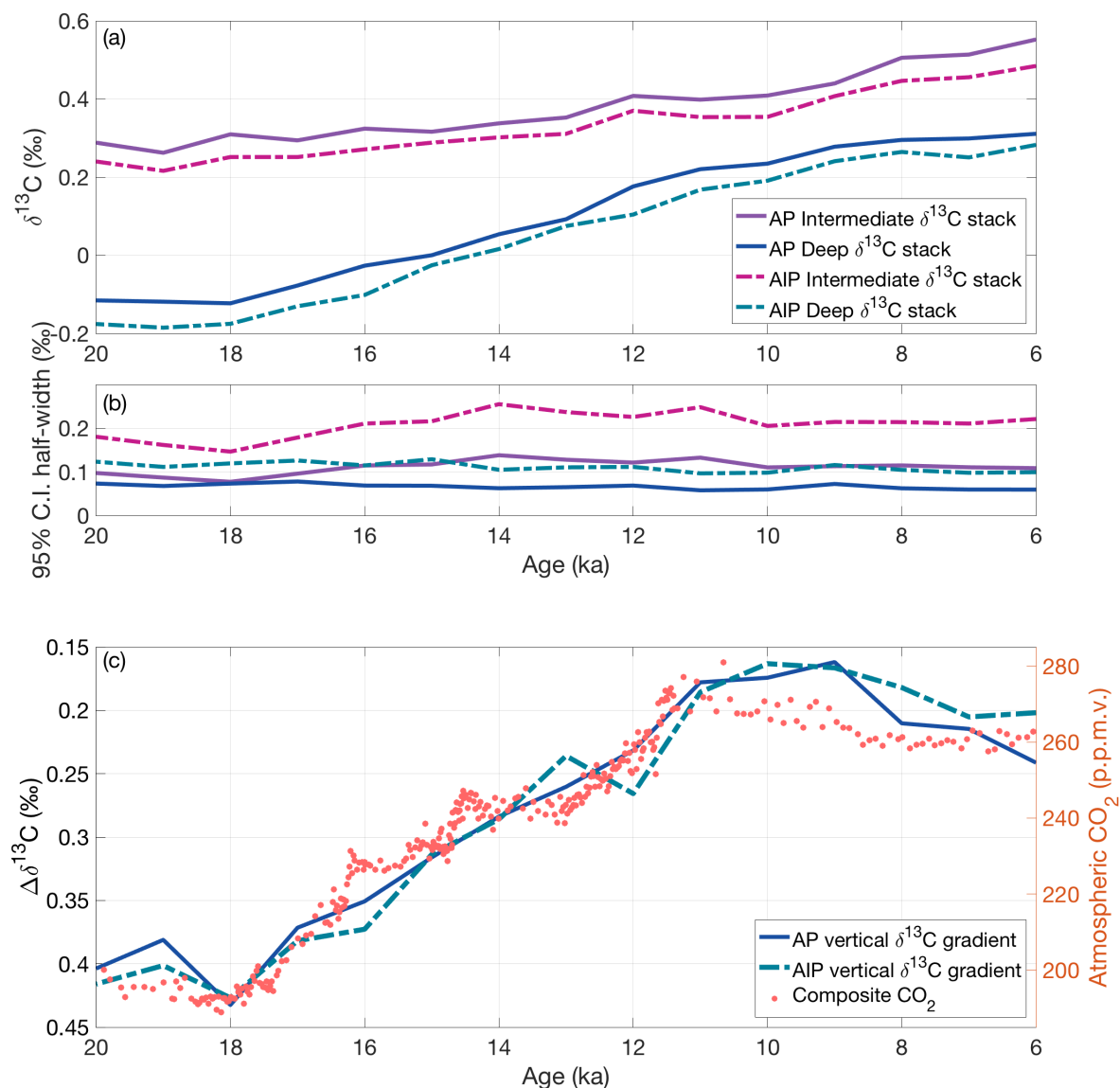


Figure A1. (a) Two versions of the deep and intermediate stacks (colors in legend) with the AIP stacks plotted in dot-dashed lines, and AP stacks plotted in solid lines. (b) The 95% C.I. half-width for each stack in the legend in figure (A1a). (c) Comparison of CO_2 and both AP and AIP vertical $\Delta\delta^{13}\text{C}$ gradients. Both volume-weighted vertical gradients closely resemble the spliced atmospheric CO_2 records (red circles) (Marcott et al., 2014; Monnin et al., 2004), but the AIP $\Delta\delta^{13}\text{C}$ gradient (dashed green-blue line) is more noisy and slightly more depleted than the AP $\Delta\delta^{13}\text{C}$ gradient (solid blue line).



Table A1. Supplemental table of the name, location, region, and reference for each record in this $\delta^{13}\text{C}$ synthesis

Core Name	Lat	Lon	Depth (m)	Region	Reference
EW9209-1JPC	5.9	-44.2	4056	LDNA	Curry and Oppo (1997)
GeoB7920-2	20.8	-18.6	2278	UDNA	Tjallingii et al. (2008)
GeoB9508-5	14.5	-17.9	2384	UDNA	Mulitza et al. (2008)
GeoB9526	12.4	-18.1	3223	UDNA	Zarriess and Mackensen (2011)
GIK17049-6	55.3	-26.7	3331	UDNA	Jung and Sarnthein (2003)
GIK17051	56.2	-31.9	2295	UDNA	Sarnthein et al. (1994)
GIK23415-9	53.2	-19.2	2472	UDNA	Weinelt et al. (2003)
KF13	37.6	-31.8	2690	UDNA	Richter (1998)
MD95-2040	40.6	-9.9	2465	UDNA	Voelker and de Abreu (2011)
MD99-2334	37.8	-10.2	3146	UDNA	Skinner and Shackleton (2004)
NA87-22	55.5	-14.7	2161	UDNA	Duplessy et al. (1992)
ODP658C	20.8	-18.6	2274	UDNA	Woodruff and Chambers (1991)
ODP980	55.5	-14.7	2168	UDNA	Oppo et al. (2006)
SU90-03	40.1	-32	2475	UDNA	Cortijo et al. (1999)
V29-202	61	-21	2658	UDNA	Oppo and Lehman (1995)
ENO66-16	5.5	-21.1	3152	UDNA	Oppo and Fairbanks (1987)
ENO66-21	4.2	-21.6	3995	UDNA	Oppo and Fairbanks (1987)
ENO66-26	3.1	-20	4745	LDNA	Oppo and Fairbanks (1987)
ENO66-32	2.5	-19.7	4998	LDNA	Oppo and Fairbanks (1987)
ENO66-36	4.3	-20.2	4095	LDNA	Oppo and Fairbanks (1987)
ENO66-38	4.9	-20.5	2931	UDNA	Oppo and Fairbanks (1987)
ENO66-44	5.3	-21.7	3428	UDNA	Oppo and Fairbanks (1987)
GeoB1101	1.7	-10.9	4588	LDNA	Bickert and Wefer (1996)
GeoB4216	30.6	-12.4	2324	UDNA	Freudenthal et al. (2002)
GIK12328-5	21.2	-18.6	2778	UDNA	Sarnthein et al. (1994)
GIK12347-2	15.8	-17.9	2576	UDNA	Sarnthein et al. (1994)
GIK12379-3	23.1	-17.8	2136	UDNA	Sarnthein et al. (1994)
GIK12392-1	25.2	-16.9	2573	UDNA	Sarnthein et al. (1994)
GIK15612-2	44.4	-26.5	3050	UDNA	Sarnthein et al. (1994)
GIK15669	34.9	-7.8	2022	UDNA	Sarnthein et al. (1994)
GIK15672	34.9	-8.1	2460	UDNA	Sarnthein et al. (1994)
GIK16402	14.4	-20.5	4202	LDNA	Sarnthein et al. (1994)
GIK17055-1	48.2	-27.1	2558	UDNA	Sarnthein et al. (1994)
GIK23414-9	53.5	-20.3	2196	UDNA	Sarnthein et al. (1994)
GIK23416-4	51.6	-20	3616	UDNA	Jung and Sarnthein et al. (1994)
GIK23417-1	50.7	-19.4	3850	UDNA	Jung and Sarnthein (2004)



Core Name	Lat	Lon	Depth (m)	Region	Reference
GIK23418-8	52.6	-20.3	2841	UDNA	Jung and Sarnthein (2004)
IODP-U1308	49.9	-24.2	3900	UDNA	Hodell et al. (2008)
KNR110-50	4.9	-43.2	3995	UDNA	Curry et al. (1988)
KNR110-55	4.9	-42.9	4556	LDNA	Curry et al. (1988)
KNR110-58	4.8	-43	4341	LDNA	Curry et al. (1988)
KNR110-66	4.6	-43.4	3547	UDNA	Curry et al. (1988)
KNR110-71	4.4	-43.7	3164	UDNA	Curry et al. (1988)
KNR110-75	4.3	-43.4	3063	UDNA	Curry et al. (1988)
KNR110-82	4.3	-43.5	2816	UDNA	Curry et al. (1988)
KNR110-91	4.8	-43.3	3810	UDNA	Curry et al. (1988)
MD95-2039	40.6	-10.4	3381	UDNA	Schönfeld et al. (2003)
ODP928	5.5	-43.8	4012	LDNA	Curry and Oppo (2005)
SU90-39	52.5	-22	3955	UDNA	Chapman and Shackleton (1998)
V22-197	14.2	-18.6	3167	UDNA	Boyle (1992)
V23-81	54.3	-16.8	2393	UDNA	Veum et al. (1992)
V25-59	1.4	-33.5	3824	UDNA	Bertram et al. (1995)
V30-49	18.4	-21.1	3093	UDNA	Boyle (1992); Martin and Lea (1998)
CH73-139	54.7	-16.4	2209	UDNA	Bickert and Mackensen (2003)
CHN82-24	43.5	-30.7	3070	UDNA	Boyle and Keigwin (1985)
GIK13521	3	-22	4504	LDNA	Sarnthein et al. (1994)
GIK16415	9.6	-19.1	3841	UDNA	Sarnthein et al. (1994)
GIK17050	55.5	-27.9	2795	UDNA	Sarnthein et al. (1994)
HM52-43	63.5	-0.7	2781	UDNA	Veum et al. (1992)
GeoB1041	-3.5	-7.6	4033	DSA	Mackensen and Bickert (1999)
GeoB1112	-5.8	-10.8	3125	DSA	Mackensen and Bickert (1999)
GeoB1117	-3.8	-14.9	3984	DSA	Mackensen and Bickert (1999)
GeoB1118	-3.6	-16.4	4675	DSA	Mackensen and Bickert (1999)
GeoB1211	-24.5	7.5	4089	DSA	Bickert and Wefer (1999)
GeoB1214	-24.7	7.2	3210	DSA	Bickert and Wefer (1999)
GeoB1710	-23.4	11.7	2987	DSA	Schmiedl and Mackensen (1997)
MD07-3076	-44.2	-14.2	3770	DSA	Skinner et al. (2010)
ODP1089	-40.9	9.9	4621	DSA	Hodell et al. (2001)
ODP1090	-42.9	8.9	3702	DSA	Venz and Hodell (2002)
PS2498	-44.2	-14.2	3783	DSA	Hodell et al. (2003)
RC13-228	-22.3	11.2	3204	DSA	Boyle (1992)
V29-135	-19.7	8.88	2675	DSA	Sarnthein et al. (1994)
V30-40	0.2	-23.2	3706	DSA	Oppo and Fairbanks (1987)



Core Name	Lat	Lon	Depth (m)	Region	Reference
DSDP502	11.5	-79.4	1800	INA	Demenocal et al. (1992)
GeoB6718	52.2	-12.8	900	INA	Rüggeberg et al. (2005)
GIK15666-6	34.9	-7.1	803	INA	Sarnthein et al. (1994)
GIK16006-1	29.3	-11.5	796	INA	Sarnthein et al. (1994)
GIK16017	21.3	-17.8	812	INA	Sarnthein et al. (1994)
OCE205-103GGC	26.1	-78.1	965	INA	Slowey and Curry (1995)
GeoB4240	28.9	-13.2	1358	INA	Freudenthal et al. (2002)
GIK11944-2	35.6	-8.1	1765	INA	Weinelt and Sarnthein (2003)
GIK16004	29.9	-10.7	1512	INA	Sarnthein et al. (1994)
GIK16030	21.2	-18.1	1500	INA	Sarnthein et al. (1994)
GIK23419	54.9	-19.8	1491	INA	Sarnthein et al. (1994)
GIK23519	64.8	-29.6	1893	INA	Millo et al. (2006)
M35003-4	12.1	-61.2	1299	INA	Zahn and Stüber (2002)
ODP982	57.5	-15.9	1134	INA	Venz et al. (1999); Venz and Hodell (2002)
ODP983	60.4	-23.6	1984	INA	Mc Intyre et al. (1999); Raymo et al. (2004)
ODP984	61	-24	1650	INA	Raymo et al. (2004)
V28-127	11.7	-80.1	1750	INA	Oppo and Fairbanks (1990)
V28-14	64.8	-29.7	1855	INA	Boyle (1992)
RC16-84	-26.7	-43.3	2438	ISA	Oppo and Horowitz (2000)
V24-253	-26.9	-44.7	2069	ISA	Oppo and Horowitz (2000)
CHN115-70	-29.9	-35.6	2340	ISA	Curry and Lohmann (1982)
MD96-2080	-36.3	19.5	2488	ISA	Martínez-Méndez et al. (2008)
ODP1088	-41.1	13.6	2082	ISA	Hodell et al. (2003)
GeoB3104	-3.7	-37.7	767	ISA	Arz et al. (1999)
BT4	-4	10	1000	ISA	Oppo and Fairbanks (1989)
KNR159-36	-27.5	-46.5	1268	ISA	Oppo and Horowitz, 2000
RC16-119	-27.7	-46.5	1567	ISA	Oppo and Horowitz (2000)
GeoB3004	14.6	52.9	1803	II	Schmiedl and Mackensen (2006)
MD01-2378	-13.1	121.8	1783	II	Xu et al. (2008)
Orgon4-KS8	23.5	59.2	2900	DI	Sirocko (1994)
SO42-74KL	14.3	57.3	3212	DI	Sirocko et al. (1993)
MD97-2151	8.7	109.9	1598	IP	Wei et al. (2006)
FR97-GC12	-23.6	153.8	990	IP	Bostock et al. (2004)
V19-27	-0.5	-82.1	1373	IP	Mix et al. (1991)
EW9504-05	32.5	-118.1	1818	IP	Stott et al. (2000)
GIK17961-2	8.5	112.3	1795	IP	Wang et al. (1999)
MD97-2120	-45.5	174.9	1210	IP	Pahnke and Zahn (2005)



Core Name	Lat	Lon	Depth (m)	Region	Reference
NGC102	32.3	157.9	2612	DP	Ohkushi et al. (2003)
ODP807A	3.6	156.6	2804	DP	Zhang et al. (2007)
ODP846	-3.1	-90.8	3296	DP	Mix et al. (1995); Shackleton et al. (1995)
RC13-110	-0.1	-95.7	3231	DP	Mix et al. (1991)
RC13-114	-1.7	-103.6	3436	DP	Marchitto et al. (2005)
V24-109	0.4	158.8	2367	DP	Shackleton et al. (1992)
ODP1143	9.4	113.3	2772	DP	Tian et al. (2002)



Table A2. Correlation coefficients and p-values between records. The upper rows are the raw data, and the bottom rows are the pre-whitened to account for autocorrelated time series. To investigate possible leads/lags between records, we shift the atmospheric CO₂ record in 100-year increments relative to the $\delta^{13}\text{C}$ stacks and, for brevity, list only the best correlations. All p-values account for reduction in degrees of freedom due to either pre-whitening and/or time shifting.

Record 1	Record 2	CO ₂ time shift (years)	r ²	
CO ₂	API $\Delta\delta^{13}\text{C}_{I-D}$	0	-0.97	
CO ₂	API $\Delta\delta^{13}\text{C}_{I-D}$	+1000	-0.99	
CO ₂	AP $\Delta\delta^{13}\text{C}_{I-D}$	0	-0.98	
CO ₂	AP $\Delta\delta^{13}\text{C}_{I-D}$	+600	-0.98	
CO ₂	$\Delta\delta^{13}\text{C}_{(INA/2)-DP}$	0	-0.98	
CO ₂	$\Delta\delta^{13}\text{C}_{(INA/2)-DP}$	-200	-0.98	
CO ₂	Global $\delta^{13}\text{C}$ stack	0	0.93	
CO ₂	Global $\delta^{13}\text{C}$ stack	+1000	0.95	
Record 1	Record 2	CO ₂ time shift (years)	Pre-whitened r ²	Pre-whitened p-value
CO ₂	API $\Delta\delta^{13}\text{C}_{I-D}$	0	-0.39	0.08
CO ₂	API $\Delta\delta^{13}\text{C}_{I-D}$	+900	-0.80	0.0003
CO ₂	AP $\Delta\delta^{13}\text{C}_{I-D}$	0	-0.70	0.002
CO ₂	AP $\Delta\delta^{13}\text{C}_{I-D}$	+300	-0.73	0.002
CO ₂	$\Delta\delta^{13}\text{C}_{(INA/2)-DP}$	0	-0.79	0.0002
CO ₂	$\Delta\delta^{13}\text{C}_{(INA/2)-DP}$	-200	-0.82	0.0002
CO ₂	Global $\delta^{13}\text{C}$ stack	0	0.20	0.24
CO ₂	Global $\delta^{13}\text{C}$ stack	-500	0.36	0.11

Clim. Past Discuss., <https://doi.org/10.5194/cp-2018-25>
Manuscript under review for journal Clim. Past
Discussion started: 15 March 2018
© Author(s) 2018. CC BY 4.0 License.



Competing interests. The authors declare that they have no conflict of interest.

Acknowledgements. We acknowledge the following colleagues whose advice and input substantially improved drafts of this manuscript: David Lea, Syee Weldeab, Jake Gebbie, Andy Ridgwell, and James Rae. Funding for this work came from NSF grants MGG 0926735 and CDI 1125181.



References

- Allen, K. A., Sikes, E. L., Hönisch, B., Elmore, A. C., Guilderson, T. P., Rosenthal, Y., and Anderson, R. F.: Southwest Pacific deep water carbonate chemistry linked to high southern latitude climate and atmospheric CO₂ during the last glacial termination, *Quaternary Science Reviews*, 122, 180–191, 2015.
- 5 Archer, D., Winguth, A., Lea, D., and Mahowald, N.: What caused the glacial/interglacial atmospheric pCO₂ cycles?, *Reviews of Geophysics* - Richmond Virginia, then Washington, 38, 159–190, 2000.
- Archer, D. E., Martin, P. A., Milovich, J., Brovkin, V., Plattner, G.-K., and Ashendel, C.: Model sensitivity in the effect of Antarctic sea ice and stratification on atmospheric pCO₂, *Paleoceanography*, 18, 2003.
- Arz, H. W., Pätzold, J., and Wefer, G.: The deglacial history of the western tropical Atlantic as inferred from high resolution stable isotope records off northeastern Brazil, *Earth and Planetary Science Letters*, 167, 105–117, 1999.
- 10 Aydin, M., Campbell, J., Fudge, T., Cuffey, K., Nicewonger, M., Verhulst, K., and Saltzman, E.: Changes in atmospheric carbonyl sulfide over the last 54,000 years inferred from measurements in Antarctic ice cores, *Journal of Geophysical Research: Atmospheres*, 2016.
- Bauska, T. K., Baggenstos, D., Brook, E. J., Mix, A. C., Marcott, S. A., Petrenko, V. V., Schaefer, H., Severinghaus, J. P., and Lee, J. E.: Carbon isotopes characterize rapid changes in atmospheric carbon dioxide during the last deglaciation, *Proceedings of the National Academy of Sciences*, 113, 3465–3470, 2016.
- 15 Bertram, C. J., Elderfield, H., Shackleton, N. J., and MacDonald, J. A.: Cadmium/calcium and carbon isotope reconstructions of the glacial northeast Atlantic Ocean, *Paleoceanography*, 10, 563–578, 1995.
- Bickert, T. and Mackensen, A.: Last Glacial to Holocene changes in South Atlantic deep water circulation, in: *The South Atlantic in the Late Quaternary*, pp. 671–693, Springer, 2003.
- 20 Bickert, T. and Wefer, G.: Late Quaternary deep water circulation in the South Atlantic: Reconstruction from carbonate dissolution and benthic stable isotopes, in: *The South Atlantic*, pp. 599–620, Springer, 1996.
- Bickert, T. and Wefer, G.: South Atlantic and benthic foraminifer $\delta^{13}\text{C}$ deviations: implications for reconstructing the Late Quaternary deep-water circulation, *Deep Sea Research Part II: Topical Studies in Oceanography*, 46, 437–452, 1999.
- Bostock, H. C., Opdyke, B. N., Gagan, M. K., and Fifield, L. K.: Carbon isotope evidence for changes in Antarctic Intermediate Water circulation and ocean ventilation in the southwest Pacific during the last deglaciation, *Paleoceanography*, 19, 2004.
- 25 Boyle, E. and Keigwin, L.: Comparison of Atlantic and Pacific paleochemical records for the last 215,000 years: Changes in deep ocean circulation and chemical inventories, *Earth and Planetary Science Letters*, 76, 135–150, 1985.
- Boyle, E. A.: Cadmium and delta ¹³C paleochemical ocean distributions during the stage 2 Glacial Maximum, *Annual Review of Earth and Planetary Sciences*, 20, 245, 1992.
- 30 Broecker, W. S.: Ocean chemistry during glacial time, *Geochimica et Cosmochimica Acta*, 46, 1689–1705, 1982.
- Brovkin, V., Ganopolski, A., Archer, D., and Rahmstorf, S.: Lowering of glacial atmospheric CO₂ in response to changes in oceanic circulation and marine biogeochemistry, *Paleoceanography*, 22, 2007.
- Brovkin, V., Ganopolski, A., Archer, D., and Munhoven, G.: Glacial CO₂ cycle as a succession of key physical and biogeochemical processes, *Climate of the Past*, 8, 251–264, 2012.
- 35 Buchanan, P. J., Matear, R. J., Lenton, A., Phipps, S. J., Chase, Z., and Etheridge, D. M.: The simulated climate of the Last Glacial Maximum and insights into the global marine carbon cycle, *Climate of the Past*, 12, 2271, 2016.
- Burke, A. and Robinson, L. F.: The Southern Ocean's role in carbon exchange during the last deglaciation, *Science*, 335, 557–561, 2012.



- Chapman, M. R. and Shackleton, N. J.: Millennial-scale fluctuations in North Atlantic heat flux during the last 150,000 years, *Earth and Planetary Science Letters*, 159, 57–70, 1998.
- Ciais, P., Tagliabue, A., Cuntz, M., Bopp, L., Scholze, M., Hoffmann, G., Lourantou, A., Harrison, S. P., Prentice, I., Kelley, D., et al.: Large inert carbon pool in the terrestrial biosphere during the Last Glacial Maximum, *Nature Geoscience*, 5, 74–79, 2012.
- 5 Cortijo, E., Lehman, S., Keigwin, L., Chapman, M., Paillard, D., and Labeyrie, L.: Changes in meridional temperature and salinity gradients in the North Atlantic Ocean (30–72 N) during the last interglacial period, *Paleoceanography*, 14, 23–33, 1999.
- Crosta, X. and Shemesh, A.: Reconciling down core anticorrelation of diatom carbon and nitrogen isotopic ratios from the Southern Ocean, *Paleoceanography*, 17, 2002.
- Curry, W. and Lohmann, G.: Carbon isotopic changes in benthic foraminifera from the western South Atlantic: Reconstruction of glacial
10 abyssal circulation patterns, *Quaternary Research*, 18, 218–235, 1982.
- Curry, W. B. and Oppo, D. W.: Synchronous, high-frequency oscillations in tropical sea surface temperatures and North Atlantic Deep Water production during the last glacial cycle, *Paleoceanography*, 12, 1–14, 1997.
- Curry, W. B. and Oppo, D. W.: Glacial water mass geometry and the distribution of $\delta^{13}\text{C}$ of ΣCO_2 in the western Atlantic Ocean, *Paleoceanography*, 20, 2005.
- 15 Curry, W. B., Duplessy, J.-C., Labeyrie, L., and Shackleton, N. J.: Changes in the distribution of $\delta^{13}\text{C}$ of deep water ΣCO_2 between the last glaciation and the Holocene, *Paleoceanography*, 3, 317–341, 1988.
- Davies-Barnard, T., Ridgwell, A., Singarayer, J., and Valdes, P.: Quantifying the Influence of the Terrestrial Biosphere on Glacial-interglacial Climate Dynamics, *Climate of the Past*, 13, 1381–1401, 2017.
- Demenocal, P. B., Oppo, D. W., Fairbanks, R. G., and Prell, W. L.: Pleistocene $\delta^{13}\text{C}$ variability of North Atlantic intermediate water,
20 *Paleoceanography*, 7, 229–250, 1992.
- Duplessy, J., Shackleton, N., Fairbanks, R., Labeyrie, L., Oppo, D., and Kallel, N.: Deepwater source variations during the last climatic cycle and their impact on the global deepwater circulation, *Paleoceanography*, 3, 343–360, 1988.
- Duplessy, J.-C., Labeyrie, L., Arnold, M., Paterne, M., Duprat, J., and van Weering, T. C.: Changes in surface salinity of the North Atlantic Ocean during the last deglaciation, *Nature*, 358, 485, 1992.
- 25 Eggleston, S., Schmitt, J., Bereiter, B., Schneider, R., and Fischer, H.: Evolution of the stable carbon isotope composition of atmospheric CO_2 over the last glacial cycle, *Paleoceanography*, 2016.
- Ferrari, R., Jansen, M. F., Adkins, J. F., Burke, A., Stewart, A. L., and Thompson, A. F.: Antarctic sea ice control on ocean circulation in present and glacial climates, *Proceedings of the National Academy of Sciences*, 111, 8753–8758, 2014.
- Flower, B. P., Oppo, D. W., McManus, J., Venz, K., Hodell, D., and Cullen, J.: North Atlantic intermediate to deep water circulation and
30 chemical stratification during the past 1 Myr, *Paleoceanography*, 15, 388, 2000.
- Franois, R., Altabet, M. A., Yu, E.-F., Sigman, D. M., Bacon, M. P., Frank, M., Bohrmann, G., Bareille, G., and Labeyrie, L. D.: Contribution of Southern Ocean surface-water stratification to low atmospheric CO_2 concentrations during the last glacial period, *Nature*, 389, 929–935, 1997.
- Freudenthal, T., Meggers, H., Henderiks, J., Kuhlmann, H., Moreno, A., and Wefer, G.: Upwelling intensity and filament activity off Morocco
35 during the last 250,000 years, *Deep Sea Research Part II: Topical Studies in Oceanography*, 49, 3655–3674, 2002.
- Galbraith, E. D. and Jaccard, S. L.: Deglacial weakening of the oceanic soft tissue pump: global constraints from sedimentary nitrogen isotopes and oxygenation proxies, *Quaternary Science Reviews*, 109, 38–48, 2015.



- Gebbie, G., Peterson, C. D., Lisiecki, L. E., and Spero, H. J.: Global-mean marine $\delta^{13}\text{C}$ and its uncertainty in a glacial state estimate, *Quaternary Science Reviews*, 125, 144–159, 2015.
- Gildor, H., Tziperman, E., and Toggweiler, J.: Sea ice switch mechanism and glacial-interglacial CO_2 variations, *Global Biogeochemical Cycles*, 16, 2002.
- 5 Gloege, L., McKinley, G. A., Mouw, C. B., and Ciochetto, A. B.: Global evaluation of particulate organic carbon flux parameterizations and implications for atmospheric pCO_2 , *Global Biogeochemical Cycles*, 31, 1192–1215, 2017.
- Gottschalk, J., Vázquez Riveiros, N., Waelbroeck, C., Skinner, L. C., Michel, E., Duplessy, J.-C., Hodell, D., and Mackensen, A.: Carbon isotope offsets between benthic foraminifer species of the genus *Cibicides* (*Cibicidoides*) in the glacial sub-Antarctic Atlantic, *Paleoceanography*, 31, 1583–1602, 2016.
- 10 Gu, S., Liu, Z., Zhang, J., Rempfer, J., Joos, F., and Oppo, D. W.: Coherent response of Antarctic Intermediate Water and Atlantic Meridional Overturning Circulation during the last deglaciation: reconciling contrasting neodymium isotope reconstructions from the tropical Atlantic, *Paleoceanography*, 32, 1036–1053, 2017.
- Herguera, J., Herbert, T., Kashgarian, M., and Charles, C.: Intermediate and deep water mass distribution in the Pacific during the Last Glacial Maximum inferred from oxygen and carbon stable isotopes, *Quaternary Science Reviews*, 29, 1228–1245, 2010.
- 15 Hertzberg, J. E., Lund, D. C., Schmittner, A., and Skrivaneck, A. L.: Evidence for a biological pump driver of atmospheric CO_2 rise during Heinrich Stadial 1, *Geophysical Research Letters*, 43, 2016.
- Hesse, T., Butzin, M., Bickert, T., and Lohmann, G.: A model-data comparison of $\delta^{13}\text{C}$ in the glacial Atlantic Ocean, *Paleoceanography*, 26, 2011.
- Hodell, D. A., Kanfoush, S. L., Shemesh, A., Crosta, X., Charles, C. D., and Guilderson, T. P.: Abrupt cooling of Antarctic surface waters and sea ice expansion in the South Atlantic sector of the Southern Ocean at 5000 cal yr BP, *Quaternary Research*, 56, 191–198, 2001.
- 20 Hodell, D. A., Venz, K. A., Charles, C. D., and Ninnemann, U. S.: Pleistocene vertical carbon isotope and carbonate gradients in the South Atlantic sector of the Southern Ocean, *Geochemistry, Geophysics, Geosystems*, 4, 1–19, 2003.
- Hodell, D. A., Channell, J. E., Curtis, J. H., Romero, O. E., and Röhl, U.: Onset of “Hudson Strait” Heinrich events in the eastern North Atlantic at the end of the middle Pleistocene transition (640 ka)?, *Paleoceanography*, 23, 2008.
- 25 Hodell, D. A., Evans, H. F., Channell, J. E., and Curtis, J. H.: Phase relationships of North Atlantic ice-rafted debris and surface-deep climate proxies during the last glacial period, *Quaternary Science Reviews*, 29, 3875–3886, 2010.
- Hoffman, J. and Lund, D.: Refining the stable isotope budget for Antarctic Bottom Water: New foraminiferal data from the abyssal southwest Atlantic, *Paleoceanography*, 27, 2012.
- Hoogakker, B., Smith, R., Singarayer, J., Marchant, R., Prentice, I., Allen, J., Anderson, R., Bhagwat, S., Behling, H., Borisova, O., et al.: Terrestrial biosphere changes over the last 120 kyr, *Climate of the Past*, 12, 51–73, 2016.
- 30 Joos, F., Gerber, S., Prentice, I., Otto-Bliesner, B. L., and Valdes, P. J.: Transient simulations of Holocene atmospheric carbon dioxide and terrestrial carbon since the Last Glacial Maximum, *Global Biogeochemical Cycles*, 18, 2004.
- Jung, S. and Sarnthein, M.: Stable isotope data of sediment cores GIK23415-9, PANGAEA, doi, 10, 2003.
- Jung, S. and Sarnthein, M.: Stable isotope analysis of foraminifera from sediment cores GIK17049-6, PANGAEA, doi, 10, 2004.
- 35 Kallel, N., Labeyrie, L. D., Juillet-Leclerc, A., and Duplessy, J.-C.: A deep hydrological front between intermediate and deep-water masses in the glacial Indian Ocean, *Nature*, 333, 651–655, 1988.
- Kaplan, J. O., Prentice, I. C., Knorr, W., and Valdes, P. J.: Modeling the dynamics of terrestrial carbon storage since the Last Glacial Maximum, *Geophysical Research Letters*, 29, 2002.



- Kerr, J., Rickaby, R., Yu, J., Elderfield, H., and Sadekov, A. Y.: The effect of ocean alkalinity and carbon transfer on deep-sea carbonate ion concentration during the past five glacial cycles, *Earth and Planetary Science Letters*, 471, 42–53, 2017.
- Kohfeld, K. E. and Chase, Z.: Temporal evolution of mechanisms controlling ocean carbon uptake during the last glacial cycle, *Earth and Planetary Science Letters*, 472, 206–215, 2017.
- 5 Kohfeld, K. E. and Ridgwell, A.: Glacial-interglacial variability in atmospheric CO₂, *Surface Ocean/Lower Atmosphere Processes, Geophysical Monograph Series*, 37, 2009.
- Köhler, P. and Fischer, H.: Simulating changes in the terrestrial biosphere during the last glacial/interglacial transition, *Global and Planetary Change*, 43, 33–55, 2004.
- Köhler, P., Joos, F., Gerber, S., and Knutti, R.: Simulated changes in vegetation distribution, land carbon storage, and atmospheric CO₂ in
10 response to a collapse of the North Atlantic thermohaline circulation, *Climate Dynamics*, 25, 689–708, 2005.
- Köhler, P., Fischer, H., and Schmitt, J.: Atmospheric $\delta^{13}\text{C}_{\text{CO}_2}$ and its relation to pCO₂ and deep ocean $\delta^{13}\text{C}$ during the late Pleistocene, *Paleoceanography*, 25, 2010.
- Lacerra, M., Lund, D., Yu, J., and Schmittner, A.: Carbon storage in the mid-depth Atlantic during millennial-scale climate events, *Paleoceanography*, 2017.
- 15 Landais, A., Lathiere, J., Barkan, E., and Luz, B.: Reconsidering the change in global biosphere productivity between the Last Glacial Maximum and present day from the triple oxygen isotopic composition of air trapped in ice cores, *Global biogeochemical cycles*, 21, 2007.
- Lisiecki, L.: Atlantic overturning responses to obliquity and precession over the last 3 Myr, *Paleoceanography*, 29, 71–86, 2014.
- Lisiecki, L. E.: A benthic $\delta^{13}\text{C}$ -based proxy for atmospheric pCO₂ over the last 1.5 Myr, *Geophysical Research Letters*, 37, n/a–n/a,
20 <https://doi.org/10.1029/2010GL045109>, <http://dx.doi.org/10.1029/2010GL045109>, 121708, 2010.
- Lisiecki, L. E., Raymo, M. E., and Curry, W. B.: Atlantic overturning responses to Late Pleistocene climate forcings, *Nature*, 456, 85–88, 2008.
- Lund, D., Adkins, J., and Ferrari, R.: Abyssal Atlantic circulation during the Last Glacial Maximum: Constraining the ratio between transport and vertical mixing, *Paleoceanography*, 26, 2011a.
- 25 Lund, D., Tessin, A., Hoffman, J., and Schmittner, A.: Southwest Atlantic water mass evolution during the last deglaciation, *Paleoceanography*, 30, 477–494, 2015.
- Lund, D. C., Mix, A. C., and Southon, J.: Increased ventilation age of the deep northeast Pacific Ocean during the last deglaciation, *Nature Geoscience*, 4, 771–774, 2011b.
- Lutze, G. and Thiel, H.: Epibenthic foraminifera from elevated microhabitats; *Cibicidoides wuellerstorfi* and *Planulina ariminensis*, *Journal*
30 *of Foraminiferal Research*, 19, 153–158, 1989.
- Lynch-Stieglitz, J., Stocker, T. F., Broecker, W. S., and Fairbanks, R. G.: The influence of air-sea exchange on the isotopic composition of oceanic carbon: Observations and modeling, *Global Biogeochemical Cycles*, 9, 653–665, 1995.
- Lynch-Stieglitz, J., Adkins, J. F., Curry, W. B., Dokken, T., Hall, I. R., Herguera, J. C., Hirschi, J. J.-M., Ivanova, E. V., Kissel, C., Marchal, O., et al.: Atlantic meridional overturning circulation during the Last Glacial Maximum, *science*, 316, 66–69, 2007.
- 35 Mackensen, A.: On the use of benthic foraminiferal $\delta^{13}\text{C}$ in palaeoceanography: constraints from primary proxy relationships, *Geological Society, London, Special Publications*, 303, 121–133, 2008.
- Mackensen, A. and Bickert, T.: Stable carbon isotopes in benthic foraminifera: proxies for deep and bottom water circulation and new production, in: *Use of proxies in paleoceanography*, pp. 229–254, Springer, 1999.



- Marchitto, T. M. and Broecker, W. S.: Deep water mass geometry in the glacial Atlantic Ocean: A review of constraints from the paleonutrient proxy Cd/Ca, *Geochemistry, Geophysics, Geosystems*, 7, 2006.
- Marchitto, T. M., Lynch-Stieglitz, J., and Hemming, S. R.: Deep Pacific CaCO₃ compensation and glacial–interglacial atmospheric CO₂, *Earth and Planetary Science Letters*, 231, 317–336, 2005.
- 5 Marcott, S. A., Bauska, T. K., Buizert, C., Steig, E. J., Rosen, J. L., Cuffey, K. M., Fudge, T., Severinghaus, J. P., Ahn, J., Kalk, M. L., et al.: Centennial-scale changes in the global carbon cycle during the last deglaciation, *Nature*, 514, 616–619, 2014.
- Marinov, I., Follows, M., Gnanadesikan, A., Sarmiento, J. L., and Slater, R. D.: How does ocean biology affect atmospheric pCO₂? Theory and models, *Journal of Geophysical Research: Oceans*, 113, 2008a.
- Marinov, I., Gnanadesikan, A., Sarmiento, J. L., Toggweiler, J., Follows, M., and Mignone, B.: Impact of oceanic circulation on biological
10 carbon storage in the ocean and atmospheric pCO₂, *Global Biogeochemical Cycles*, 22, 2008b.
- Martin, P. A. and Lea, D. W.: Comparison of water mass changes in the deep tropical Atlantic derived from Cd/Ca and carbon isotope records: Implications for changing Ba composition of deep Atlantic water masses, *Paleoceanography*, 13, 572–585, 1998.
- Martínez-García, A., Rosell-Melé, A., Geibert, W., Gersonde, R., Masqué, P., Gaspari, V., and Barbante, C.: Links between iron supply, marine productivity, sea surface temperature, and CO₂ over the last 1.1 Ma, *Paleoceanography*, 24, 2009.
- 15 Martínez-Méndez, G., Zahn, R., Hall, I. R., Pena, L. D., and Cacho, I.: 345,000-year-long multi-proxy records off South Africa document variable contributions of Northern versus Southern Component Water to the Deep South Atlantic, *Earth and Planetary Science Letters*, 267, 309–321, 2008.
- Matsumoto, K. and Lynch-Stieglitz, J.: Similar glacial and Holocene deep water circulation inferred from southeast Pacific benthic foraminiferal carbon isotope composition, *Paleoceanography*, 14, 149–163, 1999.
- 20 Matsumoto, K., Oba, T., Lynch-Stieglitz, J., and Yamamoto, H.: Interior hydrography and circulation of the glacial Pacific Ocean, *Quaternary Science Reviews*, 21, 1693–1704, 2002.
- Mc Intyre, K., Ravelo, A., and Delaney, M.: North Atlantic intermediate waters in the late Pliocene to early Pleistocene, *Paleoceanography*, 14, 324–335, 1999.
- McManus, J., Francois, R., Gherardi, J.-M., Keigwin, L., and Brown-Leger, S.: Collapse and rapid resumption of Atlantic meridional circulation linked to deglacial climate changes, *Nature*, 428, 834–837, 2004.
- 25 Menviel, L., Joos, F., and Ritz, S.: Simulating atmospheric CO₂, $\delta^{13}C$ and the marine carbon cycle during the Last Glacial–Interglacial cycle: possible role for a deepening of the mean remineralization depth and an increase in the oceanic nutrient inventory, *Quaternary Science Reviews*, 56, 46–68, 2012.
- Menviel, L., Yu, J., Joos, F., Mouchet, A., Meissner, K., and England, M.: Poorly ventilated deep ocean at the Last Glacial Maximum inferred
30 from carbon isotopes: A data-model comparison study, *Paleoceanography*, 32, 2–17, 2017.
- Millo, C., Sarnthein, M., Voelker, A., and Erlenkeuser, H.: Variability of the Denmark Strait overflow during the last glacial maximum, *Boreas*, 35, 50–60, 2006.
- Mix, A., Pisias, N., Zahn, R., Rugh, W., Lopez, C., and Nelson, K.: Carbon 13 in Pacific Deep and Intermediate Waters, 0–370 ka: Implications for Ocean Circulation and Pleistocene CO₂, *Paleoceanography*, 6, 205–226, 1991.
- 35 Mix, A. C., Pisias, N. G., Rugh, W., Wilson, J., Morey, A., and Hagelberg, T.: Benthic foraminifer stable isotope record from Site 849 (0–5 Ma): Local and global climate changes, *Proceedings of the Ocean Drilling Program, Scientific Results*, 1995.



- Monnin, E., Steig, E. J., Siegenthaler, U., Kawamura, K., Schwander, J., Stauffer, B., Stocker, T. F., Morse, D. L., Barnola, J.-M., Bellier, B., et al.: Evidence for substantial accumulation rate variability in Antarctica during the Holocene, through synchronization of CO₂ in the Taylor Dome, Dome C and DML ice cores, *Earth and Planetary Science Letters*, 224, 45–54, 2004.
- Mulitza, S., Prange, M., Stuut, J.-B., Zabel, M., von Dobeneck, T., Itambi, A. C., Nizou, J., Schulz, M., and Wefer, G.: Sahel megadroughts triggered by glacial slowdowns of Atlantic meridional overturning, *Paleoceanography*, 23, 2008.
- Ohkushi, K., Itaki, T., and Nemoto, N.: Last Glacial–Holocene change in intermediate-water ventilation in the Northwestern Pacific, *Quaternary Science Reviews*, 22, 1477–1484, 2003.
- Oliver, K. I., Hoogakker, B. A., Crowhurst, S., Henderson, G., Rickaby, R., Edwards, N., and Elderfield, H.: A synthesis of marine sediment core $\delta^{13}\text{C}$ data over the last 150 000 years, *Climate of the Past*, 6, 645–673, 2010.
- 10 Oppo, D. and Fairbanks, R.: Atlantic Ocean thermohaline circulation of the last 150,000 years: Relationship to climate and atmospheric CO₂, *Paleoceanography*, 5, 277–288, 1990.
- Oppo, D. W. and Fairbanks, R. G.: Variability in the deep and intermediate water circulation of the Atlantic Ocean during the past 25,000 years: Northern Hemisphere modulation of the Southern Ocean, *Earth and Planetary Science Letters*, 86, 1–15, 1987.
- Oppo, D. W. and Fairbanks, R. G.: Carbon isotope composition of tropical surface water during the past 22,000 years, *Paleoceanography*, 4, 15 333–351, 1989.
- Oppo, D. W. and Horowitz, M.: Glacial deep water geometry: South Atlantic benthic foraminiferal Cd/Ca and $\delta^{13}\text{C}$ evidence, *Paleoceanography*, 15, 147–160, 2000.
- Oppo, D. W. and Lehman, S. J.: Suborbital timescale variability of North Atlantic Deep Water during the past 200,000 years, *Paleoceanography*, 10, 901–910, 1995.
- 20 Oppo, D. W., McManus, J. F., and Cullen, J. L.: Evolution and demise of the Last Interglacial warmth in the subpolar North Atlantic, *Quaternary Science Reviews*, 25, 3268–3277, 2006.
- Oppo, D. W., Curry, W. B., and McManus, J. F.: What do benthic $\delta^{13}\text{C}$ and $\delta^{18}\text{O}$ data tell us about Atlantic circulation during Heinrich Stadial 1?, *Paleoceanography*, 30, 353–368, 2015.
- Pahnke, K. and Zahn, R.: Southern Hemisphere water mass conversion linked with North Atlantic climate variability, *Science*, 307, 1741–25 1746, 2005.
- Paillard, D. and Parrenin, F.: The Antarctic ice sheet and the triggering of deglaciations, *Earth and Planetary Science Letters*, 227, 263–271, 2004.
- Peacock, S., Lane, E., and Restrepo, J. M.: A possible sequence of events for the generalized glacial-interglacial cycle, *Global Biogeochemical Cycles*, 20, 2006.
- 30 Peterson, C. D., Lisiecki, L. E., and Stern, J. V.: Deglacial whole-ocean $\delta^{13}\text{C}$ change estimated from 480 benthic foraminiferal records, *Paleoceanography*, 29, 549–563, 2014.
- Raymo, M. E., Oppo, D. W., Flower, B. P., Hodell, D., McManus, J. F., Venz, K., Kleiven, K., and McIntyre, K.: Stability of North Atlantic water masses in face of pronounced climate variability during the Pleistocene, *Paleoceanography*, 19, 2004.
- Richter, T.: Sedimentary fluxes at the mid-atlantic ridge-sediment sources, accumulation rates, and geochemical characterisation, GEOMAR Report, GEOMAR Research Center for Marine Geosciences, Christian Albrechts University in Kiel, 73, 173, 1998.
- 35 Ruddiman, W. F. and Ellis, E. C.: Effect of per-capita land use changes on Holocene forest clearance and CO₂ emissions, *Quaternary Science Reviews*, 28, 3011–3015, 2009.



- Rüggeberg, A., Dorschel, B., Dullo, W.-C., and Hebbeln, D.: Sedimentary patterns in the vicinity of a carbonate mound in the Hovland Mound Province, northern Porcupine Seabight, in: *Cold-water Corals and Ecosystems*, pp. 87–112, Springer, <https://doi.org/10.1594/PANGAEA.711998>, 2005.
- Sarnthein, M., Winn, K., Jung, S. J., Duplessy, J.-C., Labeyrie, L., Erlenkeuser, H., and Ganssen, G.: Changes in east Atlantic deepwater circulation over the last 30,000 years: Eight time slice reconstructions, *Paleoceanography*, 9, 209–267, 1994.
- Schmiedl, G. and Mackensen, A.: Late Quaternary paleoproductivity and deep water circulation in the eastern South Atlantic Ocean: Evidence from benthic foraminifera, *Palaeogeography, Palaeoclimatology, Palaeoecology*, 130, 43–80, 1997.
- Schmiedl, G. and Mackensen, A.: Multispecies stable isotopes of benthic foraminifera reveal past changes of organic matter decomposition and deepwater oxygenation in the Arabian Sea, *Paleoceanography*, 21, 2006.
- Schmitt, J., Schneider, R., Elsig, J., Leuenberger, D., Lourantou, A., Chappellaz, J., Köhler, P., Joos, F., Stocker, T. F., Leuenberger, M., et al.: Carbon isotope constraints on the deglacial CO₂ rise from ice cores, *Science*, 336, 711–714, 2012.
- Schmittner, A., Bostock, H. C., Cartapanis, O., Curry, W. B., Filipsson, H. L., Galbraith, E. D., Gottschalk, J., Herguera, J. C., Hoogakker, B., Jaccard, S., et al.: Calibration of the Carbon Isotope Composition ($\delta^{13}\text{C}$) of Benthic Foraminifera, *Paleoceanography*, 32, 512–530, 2017.
- Schönfeld, J., Zahn, R., and de Abreu, L.: Surface and deep water response to rapid climate changes at the Western Iberian Margin, *Global and Planetary Change*, 36, 237–264, 2003.
- Schweizer, M., Pawlowski, J., Kouwenhoven, T., and van der Zwaan, B.: Molecular phylogeny of common cibicidids and related Rotaliida (Foraminifera) based on small subunit rDNA sequences, *The Journal of Foraminiferal Research*, 39, 300–315, 2009.
- Shackleton, N.: Carbon-13 in *Uvigerina*: Tropical rainforest history and the equatorial Pacific carbonate dissolution cycles, *Marine science*, 1977.
- Shackleton, N., Le, J., Mix, A., and Hall, M.: Carbon isotope records from Pacific surface waters and atmospheric carbon dioxide, *Quaternary Science Reviews*, 11, 387–400, 1992.
- Shackleton, N., Hall, M., and Pate, D.: 15. Pliocene stable isotope stratigraphy of Site 846, in: *Proc. Ocean Drill. Program Sci. Results*, vol. 138, pp. 337–355, 1995.
- Shackleton, N. J., Imbrie, J., and Hall, M.: Oxygen and carbon isotope record of East Pacific core V19-30: implications for the formation of deep water in the late Pleistocene North Atlantic, *Earth and Planetary Science Letters*, 65, 233–244, 1983.
- Siegenthaler, U., Stocker, T. F., Monnin, E., Lüthi, D., Schwander, J., Stauffer, B., Raynaud, D., Barnola, J.-M., Fischer, H., Masson-Delmotte, V., et al.: Stable carbon cycle–climate relationship during the late Pleistocene, *Science*, 310, 1313–1317, 2005.
- Sigman, D. M. and Boyle, E. A.: Glacial/interglacial variations in atmospheric carbon dioxide, *Nature*, 407, 859–869, 2000.
- Sikes, E. L., Cook, M. S., and Guilderson, T. P.: Reduced deep ocean ventilation in the Southern Pacific Ocean during the last glaciation persisted into the deglaciation, *Earth and Planetary Science Letters*, 438, 130–138, 2016.
- Sikes, E. L., Allen, K. A., and Lund, D. C.: Enhanced $\delta^{13}\text{C}$ and $\delta^{18}\text{O}$ Differences Between the South Atlantic and South Pacific During the Last Glaciation: The Deep Gateway Hypothesis, *Paleoceanography*, 32, 1000–1017, 2017.
- Sirocko, F.: Abrupt change in monsoonal climate: evidence from the geochemical composition of Arabian Sea sediments, Ph.D. thesis, Christian-Albrechts-Universität zu Kiel, 1994.
- Sirocko, F., Sarnthein, M., Erlenkeuser, H., Lange, H., Arnold, M., and Duplessy, J. C.: Century-scale events in monsoonal climate over the past 24,000 years, *Nature*, 364, 322, 1993.



- Skinner, L. and Shackleton, N.: Rapid transient changes in northeast Atlantic deep water ventilation age across Termination I, *Paleoceanography*, 19, 2004.
- Skinner, L., Fallon, S., Waelbroeck, C., Michel, E., and Barker, S.: Ventilation of the deep Southern Ocean and deglacial CO₂ rise, *Science*, 328, 1147–1151, 2010.
- 5 Skinner, L. C., Primeau, F., Freeman, E., de la Fuente, M., Goodwin, P., Gottschalk, J., Huang, E., McCave, I., Noble, T., and Scrivner, A.: Radiocarbon constraints on the glacial ocean circulation and its impact on atmospheric CO₂, *Nature communications*, 8, 16010, 2017.
- Slowey, N. C. and Curry, W. B.: Glacial-interglacial differences in circulation and carbon cycling within the upper western North Atlantic, *Paleoceanography*, 10, 715–732, 1995.
- Stern, J. V. and Lisiecki, L. E.: Termination 1 timing in radiocarbon-dated regional benthic $\delta^{18}\text{O}$ stacks, *Paleoceanography*, 29, 1127–1142,
10 2014.
- Stott, L. D., Neumann, M., and Hammond, D.: Intermediate water ventilation on the northeastern Pacific margin during the late Pleistocene inferred from benthic foraminiferal $\delta^{13}\text{C}$, *Paleoceanography*, 15, 161–169, 2000.
- Talley, L. D.: Closure of the global overturning circulation through the Indian, Pacific, and Southern Oceans: Schematics and transports, *Oceanography*, 26, 80–97, 2013.
- 15 Tessin, A. and Lund, D.: Isotopically depleted carbon in the mid-depth South Atlantic during the last deglaciation, *Paleoceanography*, 28, 296–306, 2013.
- Thornalley, D. J., Elderfield, H., and McCave, I. N.: Intermediate and deep water paleoceanography of the northern North Atlantic over the past 21,000 years, *Paleoceanography*, 25, 2010.
- Tian, J., Wang, P., Cheng, X., and Li, Q.: Astronomically tuned Plio–Pleistocene benthic $\delta^{18}\text{O}$ record from South China Sea and Atlantic–
20 Pacific comparison, *Earth and Planetary Science Letters*, 203, 1015–1029, 2002.
- Tjallingii, R., Claussen, M., Stuut, J.-B. W., Fohlmeister, J., Jahn, A., Bickert, T., Lamy, F., and Röhl, U.: Coherent high- and low-latitude control of the northwest African hydrological balance, *Nature Geoscience*, 1, 670, 2008.
- Toggweiler, J., Russell, J. L., and Carson, S.: Midlatitude westerlies, atmospheric CO₂, and climate change during the ice ages, *Paleoceanography*, 21, 2006.
- 25 Vecsei, A. and Berger, W. H.: Increase of atmospheric CO₂ during deglaciation: constraints on the coral reef hypothesis from patterns of deposition, *Global Biogeochemical Cycles*, 18, 2004.
- Venz, K. A. and Hodell, D. A.: New evidence for changes in Plio–Pleistocene deep water circulation from Southern Ocean ODP Leg 177 Site 1090, *Palaeogeography, Palaeoclimatology, Palaeoecology*, 182, 197–220, 2002.
- Venz, K. A., Hodell, D. A., Stanton, C., and Warnke, D. A.: A 1.0 Myr record of Glacial North Atlantic Intermediate Water variability from
30 ODP site 982 in the northeast Atlantic, *Paleoceanography*, 14, 42–52, 1999.
- Veum, T., Jansen, E., Arnold, M., Beyer, I., and Duplessy, J.-C.: Water mass exchange between the North Atlantic and the Norwegian Sea during the past 28,000 years, *Nature*, 356, 783, 1992.
- Voelker, A. H. and de Abreu, L.: A review of abrupt climate change events in the Northeastern Atlantic Ocean (Iberian Margin): Latitudinal, longitudinal, and vertical gradients, *Abrupt Climate Change: Mechanisms, Patterns, and Impacts*, pp. 15–37, 2011.
- 35 Waelbroeck, C., Skinner, L., Labeyrie, L., Duplessy, J.-C., Michel, E., Vazquez Riveiros, N., Gherardi, J.-M., and Dewilde, F.: The timing of deglacial circulation changes in the Atlantic, *Paleoceanography*, 26, 2011.
- Wagner, M. and Hendy, I. L.: Trace metal evidence for a poorly ventilated glacial Southern Ocean, *Quaternary Science Reviews*, 170, 109–120, 2017.



- Wang, L., Sarnthein, M., Erlenkeuser, H., Grimalt, J., Grootes, P., Heilig, S., Ivanova, E., Kienast, M., Pelejero, C., and Pflaumann, U.: East Asian monsoon climate during the Late Pleistocene: high-resolution sediment records from the South China Sea, *Marine Geology*, 156, 245–284, 1999.
- Wei, G.-J., Huang, C.-Y., Wang, C.-C., Lee, M.-Y., and Wei, K.-Y.: High-resolution benthic foraminifer $\delta^{13}\text{C}$ records in the South China Sea during the last 150 ka, *Marine Geology*, 232, 227–235, 2006.
- Weinelt, M. and Sarnthein, M.: Stable isotope analysis on sediment core GIK11944-2, PANGAEA, doi: 10.1594/PANGAEA.97104 Reference (s): Weinelt, Mara (1993): Veränderungen der Oberflächenzirkulation im Europäischen Nordmeer während der letzten 60.000 Jahre-Hinweise aus stabilen Isotopen, *Berichte aus dem Sonderforschungsbereich 313*, Christian-Albrechts-Universität, Kiel, 41, 106, 2003.
- 10 Weinelt, M., Vogelsang, E., Kucera, M., Pflaumann, U., Sarnthein, M., Voelker, A., Erlenkeuser, H., and Malmgren, B.: Variability of North Atlantic heat transfer during MIS 2, *Paleoceanography*, 18, 2003.
- Woodruff, F. and Chambers, S.: Middle Miocene benthic foraminiferal oxygen and carbon isotopes and stratigraphy: southern ocean site 744, in: *Proc. ODP Sci. Results*, vol. 119, pp. 935–939, 1991.
- Woodruff, F. and Savin, S. M.: $\delta^{13}\text{C}$ values of Miocene Pacific benthic foraminifera: Correlations with sea level and biological productivity, *Geology*, 13, 119–122, 1985.
- 15 Xu, J., Holbourn, A., Kuhnt, W., Jian, Z., and Kawamura, H.: Changes in the thermocline structure of the Indonesian outflow during Terminations I and II, *Earth and Planetary Science Letters*, 273, 152–162, 2008.
- Yu, J., Anderson, R., and Rohling, E.: Deep ocean carbonate chemistry and glacial-interglacial atmospheric CO_2 changes, *Oceanography*, 2014.
- 20 Zahn, R. and Stüber, A.: Suborbital intermediate water variability inferred from paired benthic foraminiferal Cd/Ca and $\delta^{13}\text{C}$ in the tropical West Atlantic and linking with North Atlantic climates, *Earth and Planetary Science Letters*, 200, 191–205, 2002.
- Zahn, R., Winn, K., and Sarnthein, M.: Benthic foraminiferal $\delta^{13}\text{C}$ and accumulation rates of organic carbon: *Uvigerina peregrina* group and *Cibicides wuellerstorfi*, *Paleoceanography*, 1, 27–42, 1986.
- Zarriess, M. and Mackensen, A.: Testing the impact of seasonal phytodetritus deposition on $\delta^{13}\text{C}$ of epibenthic foraminifer *Cibicides wuellerstorfi*: A 31,000 year high-resolution record from the northwest African continental slope, *Paleoceanography*, 26, 2011.
- 25 Zhang, J., Wang, P., Li, Q., Cheng, X., Jin, H., and Zhang, S.: Western equatorial Pacific productivity and carbonate dissolution over the last 550 kyr: Foraminiferal and nannofossil evidence from ODP Hole 807A, *Marine Micropaleontology*, 64, 121–140, 2007.